



This is a repository copy of *Manganese Tricarbonyl Complexes with Asymmetric 2-Iminopyridine Ligands: Toward Decoupling Steric and Electronic Factors in Electrocatalytic CO₂ Reduction.*

White Rose Research Online URL for this paper:
<http://eprints.whiterose.ac.uk/112705/>

Version: Accepted Version

Article:

Spall, S.J.P., Keane, T. orcid.org/0000-0003-4975-0868, Tory, J. et al. (6 more authors) (2016) Manganese Tricarbonyl Complexes with Asymmetric 2-Iminopyridine Ligands: Toward Decoupling Steric and Electronic Factors in Electrocatalytic CO₂ Reduction. *Inorganic Chemistry*, 55 (24). pp. 12568-12582. ISSN 0020-1669

<https://doi.org/10.1021/acs.inorgchem.6b01477>

Reuse

Unless indicated otherwise, fulltext items are protected by copyright with all rights reserved. The copyright exception in section 29 of the Copyright, Designs and Patents Act 1988 allows the making of a single copy solely for the purpose of non-commercial research or private study within the limits of fair dealing. The publisher or other rights-holder may allow further reproduction and re-use of this version - refer to the White Rose Research Online record for this item. Where records identify the publisher as the copyright holder, users can verify any specific terms of use on the publisher's website.

Takedown

If you consider content in White Rose Research Online to be in breach of UK law, please notify us by emailing eprints@whiterose.ac.uk including the URL of the record and the reason for the withdrawal request.



eprints@whiterose.ac.uk
<https://eprints.whiterose.ac.uk/>

Manganese tricarbonyl complexes with asymmetric 2-imino-pyridine ligands: towards decoupling steric and electronic factors in electrocatalytic CO₂ reduction

Steven J. P. Spall,¹ Theo Keane,¹ Joanne Tory,² Dean C. Cocker,¹ Harry Adams,¹ Hannah Fowler,¹ Anthony J. H. M. Meijer,¹ František Hartl^{2*} and Julia A. Weinstein^{1*}

¹Department of Chemistry, University of Sheffield, Sheffield, S3 7HF, UK;

²Department of Chemistry, University of Reading, Whiteknights, Reading RG6 6AD, UK

KEYWORDS: CO₂ reduction, transition metal complexes, Mn complexes, IR spectroelectrochemistry

ABSTRACT: Manganese tricarbonyl bromide complexes incorporating IP (2-[(phenylimino)]pyridine) derivatives, [MnBr(CO)₃(IP)], are demonstrated as a new group of catalysts for CO₂ reduction, which represent the first example of utilization of phenylimino pyridine ligands on manganese centers for this purpose. The key feature is the asymmetric structure of the redox non-innocent ligand that permits independent tuning of its steric and electronic properties. The α -diimine ligands and five new Mn(I) compounds have been synthesized, isolated in high yields and fully characterized, including X-ray crystallography. Their electrochemical and electrocatalytic behavior was investigated using cyclic voltammetry and UV-vis /IR spectroelectrochemistry within an OTTL cell. Mechanistic investigations under an inert atmosphere have revealed differences in the nature of the reduction products as a function of steric bulk of the ligand. The direct ECE (electrochemical-chemical-electrochemical) formation of a five-coordinate anion [Mn(CO)₃(IP)]⁻, a product of 2-electron reduction of the parent complex, is observed in case of the bulky DIPIMP (2-[(2,6-diisopropyl-phenylimino)-methyl]-pyridine), TBIMP (2-[[2-¹butyl-phenylimino)-methyl]pyridine) and TBIEP (2-[[2-¹butyl-phenylimino)-ethyl]pyridine) derivatives. This process is replaced for the least sterically demanding IP ligand in [MnBr(CO)₃(IMP)] (2-[(phenylimino)-methyl]-pyridine) by the stepwise formation of such monoanion via an ECEC(E) mechanism involving also the intermediate Mn–Mn dimer, [Mn(CO)₃(IMP)]₂. The complex [MnBr(CO)₃(IPIMP)] (2-[(2-diisopropyl-phenylimino)-methyl]-pyridine), which carries a moderately electron-donating, moderately bulky IP ligand, shows an intermediate behavior where both the 5-coordinate anion and its dimeric precursor are jointly detected on the timescale of the spectroelectrochemical experiments. Under the atmosphere of CO₂ the studied complexes, except the DIPIMP derivative, rapidly coordinate CO₂, forming stable bicarbonate intermediates, with no dimer being observed. Such behavior indicates that the CO₂-binding is outcompeting another pathway, viz. the dimerization reaction between the 5-coordinate anion and the neutral parent complex. The bicarbonate intermediate species undergo reduction at more negative potentials (ca. -2.2 V vs Fc/Fc⁺), recovering [Mn(CO)₃(IP)]⁻ and triggering the catalytic production of CO.

The interest in solar fuels in terms of both photocatalytic and electrocatalytic CO₂ reduction¹, in the latter case utilizing sustainable electricity, has been increasing markedly in the new millennium. The recent demonstration of the electrocatalytic activity of manganese² analogues of the archetypal Re(I) catalysts^{3,4,5,6} for CO₂ reduction has given a new impetus to research into noble-metal-free catalytic systems. [MnBr(CO)₃(α -diimine)] complexes have been shown to outperform rhenium-based analogues with regard to CO₂ reduction under certain conditions.⁷ Most notably, the presence of a Brønsted acid⁷⁻¹⁰ appears to be a prerequisite for catalysis with a range of tricarbonyl Mn α -diimine complexes.

Mechanistic studies^{5,10} of the active 2,2'-bipyridine-based (R-bpy) manganese catalysts have shown that one-electron reduction of the parent complex [MnBr(CO)₃(R-bpy)] precursor results in the formation of the Mn–Mn dimer [Mn(CO)₃(R-bpy)]₂.^{8,9} Notably, neither the primary reduction product [MnBr(CO)₃(R-bpy)^{•-}] nor the five-coordinate radical interme-

diates [Mn(CO)₃(R-bpy)][•] have been detected by either UV-vis or IR spectroscopy.^{2,7} Nanosecond time-resolved infrared (TRIR) studies reveal that no detectable solvent adduct is formed before the dimerization of Mn species on this timescale; instead, the five-coordinate species is observed, which rapidly dimerises.¹⁰ For some of the Re analogues, a one-electron reduced complex, [ReCl(CO)₃(R-bpy)^{•-}] was observed by IR spectroscopy and identified by the ca. 15-20 cm⁻¹ decrease in the $\tilde{\nu}$ (CO) energy,^{11,12,13} as was the five-coordinate radical [Re(CO)₃(R-bpy)][•] by an additional 15-20 cm⁻¹ shift.

Two mechanisms have been proposed^{10,14-18} for the ultimate reduction of [Mn(CO)₃(α -diimine)]₂ in the presence of CO₂, which can be referred to as the anionic, and the oxidative addition¹⁹ pathways. The anionic pathway involves reduction of the dimer [Mn(CO)₃(α -diimine)]₂ at a more negative potential than the parent complex generating the five-coordinate anion [Mn(CO)₃(α -diimine)]⁻ to which CO₂ coordinates and is catalyti-

cally reduced in the presence of a Brønsted acid (the source of H^+). The anionic pathway is broadly similar to the two-electron pathway observed for Re complexes.^{20,21} In contrast, the uncommon second pathway identified using pulsed EPR studies¹⁹ involves coordination of CO_2 to the dimer $[Mn(CO)_3(2,2'-bpy)]_2$ in the presence of a Brønsted acid in a concerted oxidative addition step. This process is shown to generate a low-spin Mn^{II} -COOH complex, from which CO is subsequently released.

Since the catalytic CO_2 reduction with the use of $[MnX(CO)_3(\alpha\text{-diimine})]$ ($\alpha\text{-diimine} = R\text{-bpy}$; X halide or pseudohalide) has been shown to proceed in many cases via a dimerization step, immobilization of the catalyst²² or introducing sterically hindering groups at bpy may have a profound effect on the catalytic activity.²³ Indeed, it has recently been shown that the use of bipyridines incorporating bulky groups in the 6,6'-positions^{24,25} (or, another bulkier heterocyclic ligand²⁶) largely inhibits dimerization in the catalytic cycle. The result is the formation of the stable 5-coordinate anion via the two-electron transfer (ECE) at the first cathodic wave. However, coordination of CO_2 to the 5-coordinate anion produces a stable species which must be reduced at considerably more negative potentials²⁷ in order for catalysis to be observed. It has recently been shown that in the presence of a Lewis acid, Mg^{2+} ,^{7,28} the catalytic overpotential²⁹ is decreased by approximately 400 mV.

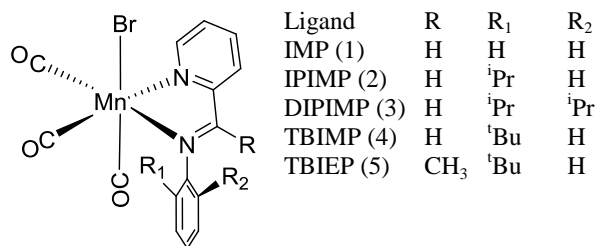


Chart 1. General structure of the complexes with the asymmetric α -diimine ligands, (2- R_1 -6- R_2 -phenyl)-(R-imino)-pyridine. Numbers given in parentheses correspond to the Mn-complexes. When R = H, the ligands will be derivatives of phenyl-iminomethyl-pyridine), IMP ($R_{1,2} = H$), IPIMP ($R_1 = {}^iPr$, $R_2 = H$), and DIPIMP ($R_{1,2} = {}^iPr$), TBIMP ($R_1 = {}^tBu$, $R_2 = H$). R = CH_3 gives TBIEP, ^tBu-phenylimino-ethyl-pyridine.

A similar behavior was observed for $[MnBr(CO)_3(R\text{-DAB})]$ complexes featuring non-aromatic 1,4-diazabuta-1,3-diene (R-DAB)^{8,9,30} ligands. The reduction potentials of the dimers $[Mn(CO)_3(R\text{-DAB})]_2$ are almost identical to those of the parent complexes, implying that the five-coordinate anion is produced directly upon reduction and reacts readily with CO_2 in solution to form a stable bicarbonate complex^{8,30} and, as with sterically hindered 2,2'-bipyridine ligands,²⁵ a much more negative potential (below 2 V vs. Fc/Fc^+) must be applied to trigger catalytic CO_2 reduction. Functionalization of the α -diimine with a sterically bulky group such as ^tBu should also modify the electronic properties of the ligand. In particular, this change should affect the energy of the LUMO, the reduction potential, and catalytic activity.²³⁻³³

Introducing steric bulk^{23,25} to prevent unwanted reactions of the catalytic species, including dimerization as either Mn-Mn,⁹ or C(imino)-C(imino) bound species,²¹ whilst at the same time reducing the risk of increased overpotential is a challenging task. Molecu-

lar designs that allow for steric and electronic effects to be decoupled are required.

In this paper we have investigated a family of tricarbonyl manganese complexes featuring asymmetric α -diimine ligands, imino-pyridines (IP).^{21,23,34,35} They combine an accessible $C=N$ imino bond of the diazabuta-1,3-diene derivatives DAB,³² with the aromatic pyridine part, thereby being a "hybrid" of 2,2'-bipyridine ligands and non-aromatic R-DAB ligands. Each of the parts is important: for instance, a Mn(I) complex with Ph-DAB demonstrates formation of 5-coordinate anions, with the steric bulk of the ligand preventing dimerization, but does not act as a catalyst for CO_2 reduction due to insufficiently negative reduction potential.⁸

Introduction of the pyridine moiety allows one to reach the required reduction potentials, whilst the Ph group attached to the $C=N$ fragment can be decorated by sterically demanding substituents, ensuring steric bulk whilst only slightly affecting the electronic properties. As the phenyl moiety lies out-of-plane with the conjugated α -diimine (because of steric effects), the π -electrons of the phenyl substituent are decoupled from the metallacycle formed by the metal center and the α -diimine. Therefore, functionalisation of the phenyl ring in the R_1 and R_2 positions with large sterically hindering groups (that also have a +I effect) will have only very minimal effects on the electronics of the active site of the molecule (vide infra). These ligands offer an opportunity to a certain extent separate steric and electronic effects in a chelating α -diimine ligand. Thus, the possibility arises of a systematic variation of the steric hindrance by changing R_1 and R_2 groups, whilst the R-group strongly influences the electronics (but could also hinder the $C=N$ bond).

These ligands are readily accessible via simple synthetic routes, which are suitable for the purpose of comparatively independent alteration of steric and electronic effects (Chart 1). The potential of such ligands³⁴⁻³⁸ has been convincingly illustrated by the recent work on a Re tricarbonyl complex with 2-(2-cyclohexyl-1-methyl)-methylimino-pyridine³⁶ (both the one-electron reduced parent complex, and the neutral 5-coordinate $Re(0)$ species were detected), and Mo pyridine-monoimides.³⁴

Herein we report a new series of manganese-based catalysts for CO_2 reduction. We will show that a change in the structure of the ligands within the same series affects the efficiency of the process, and the relative distribution of the intermediate species, demonstrating the versatile and tuneable nature of this type of catalysts.

Experimental

All solvents were supplied by VWR and used as received. The compounds were purchased from either Sigma-Aldrich or STREM Chemicals and, unless stated, used as received. Tetrabutylammonium hexafluorophosphate, $[Bu_4N][PF_6]$ was recrystallized from hot ethanol and dried overnight in a vacuum oven before use in the electrochemical studies. TBIEP (2-[^tBu-phenyl-imino)-ethyl] pyridine) and TBIMP were synthesized as previously described,³⁵ the analytical data matched that reported previously. Unless otherwise stated, UV-vis spectra were recorded on a Carry 50 Bio spectrophotometer, and IR spectra on a Perkin Elmer Spectrum 1 FT-IR spectrometer.

Syntheses

IMP (2-[(phenylimino)methyl]pyridine)

Aniline (11.3 mmol, 1.05 g, 1.02 ml) was added to 2-pyridine carboxaldehyde (11.3 mmol, 1.2 g, 1.1 ml) in flame-dried glassware and stirred for 1 h. Hexane (10 ml) was added and the solution dried over sodium sulfate. The solution was filtered, concentrated under vacuum, and placed in a freezer overnight. Large yellow needle-like crystals formed were filtered and washed with hexane. Yield 73 %. $^1\text{H NMR}$ (400 MHz, CDCl_3) δ 8.72 (d, $J = 4.7$ Hz, 1H), 8.61 (s, 1H), 8.21 (d, $J = 7.9$ Hz, 1H), 7.83 (td, $J = 7.7, 1.6$ Hz, 1H), 7.47 – 7.35 (m, 3H), 7.29 (d, $J = 7.7$ Hz, 3H), 1.58 (s, 4H).

IPIMP (2-[2-isopropylphenylimino)methyl]pyridine)

2-isopropylaniline (12.4 mmol, 1.7 g, 1.8 ml) was mixed with 2-pyridine carboxaldehyde (12.4 mmol, 1.3 g, 1.2 ml) in flame-dried glassware and stirred for 1 h. Hexane (20 ml) was added and the solution dried over sodium sulfate. The solution was filtered and solvent removed under vacuum, yielding the product as a brown oil. Previous reports indicated that this compound could not be crystallized therefore, the oil was used in the next reaction step without further purification (purity by NMR > 97 %).

$^1\text{H NMR}$ (400 MHz, CDCl_3) δ 8.72 (ddd, $J = 4.8, 1.6, 0.9$ Hz, 1H), 8.54 (s, 1H), 8.26 (dd, $J = 7.9, 0.9$ Hz, 1H), 7.82 (ddd, $J = 7.9, 1.7, 0.8$ Hz, 1H), 7.45 – 7.32 (m, 2H), 7.31 – 7.22 (m, 2H), 7.08 – 6.96 (m, 1H), 3.56 (dp, $J = 13.8, 6.8$ Hz, 1H), 1.26 (dd, $J = 6.8, 4.1$ Hz, 7H).

DIPIMP (2-[(2,6-diisopropylphenylimino)-Me]-pyridine)

2,6-diisopropylaniline (11.3 mmol, 2 g, 2.1 ml) was mixed with 2-pyridine carboxaldehyde (11.3 mmol, 1.2 g, 1.1 ml) in flame-dried glassware and stirred for 2 h. Hexane (10 ml) was added and the solution dried over sodium sulfate. The solution was filtered and concentrated before having been placed in a freezer overnight. Light brown to yellow crystals were formed, which were filtered off and washed with hexane. Yield 67 %. $^1\text{H NMR}$ (400 MHz, CDCl_3) δ 8.73 (ddd, $J = 4.8, 1.7, 0.9$ Hz, 1H), 8.31 (s, 1H), 8.27 (dt, $J = 7.9, 1.0$ Hz, 1H), 7.90 – 7.82 (m, 1H), 7.42 (ddd, $J = 7.5, 4.9, 1.2$ Hz, 1H), 7.22 – 7.07 (m, 3H), 2.97 (hept, $J = 6.9$ Hz, 2H), 1.62 (s, 1H), 1.18 (d, $J = 6.9$ Hz, 13H).

Complexes **1-6** were prepared from $[\text{MnBr}(\text{CO})_5]$ and the corresponding ligand, using diethyl ether as a solvent. The products were collected by centrifugation, and washed with diethyl ether to afford analytically pure **1-6**. $^1\text{H NMR}$ spectra for **1-5** are given in Fig. SI 22-26.

$[\text{MnBr}(\text{CO})_3(\text{IMP})]$ (**1**)

$[\text{MnBr}(\text{CO})_5]$ (1.1 mmol, 0.3 g) was combined with IMP (1.1 mmol, 0.2 g) in diethyl ether (20 ml) and refluxed under aerobic conditions for 4 h.³⁹ Product was formed in quantitative yield. $^1\text{H NMR}$ (500 MHz, CDCl_3) δ 9.26 (d, $J = 5.0$ Hz, 1H), 8.45 (s, $J = 27.9$ Hz, 1H), 8.14 – 7.79 (m, 3H), 7.68 – 7.36 (m, 5H). HRMS (TOF-ESI, +ve): m/z ($\text{M}+\text{Na}^+$) Calcd for $\text{C}_{15}\text{H}_{10}\text{N}_2\text{O}_3\text{NaBrMn}$ 422.9153; Found 422.9149.

$[\text{MnBr}(\text{CO})_3(\text{IPIMP})]$ (**2**)

$[\text{MnBr}(\text{CO})_5]$ (0.89 mmol, 0.24 g) was combined with IPIMP (0.89 mmol, 0.2 g) in diethyl ether (20 ml) and refluxed under aerobic conditions for 4 h. The product was formed in quantita-

ive yield. $^1\text{H NMR}$ (500 MHz, CDCl_3) δ 9.27 (s, 1H), 8.39 (s, 1H), 8.04 (s, 1H), 7.94 (d, $J = 4.1$ Hz, 1H), 7.78 (d, $J = 7.0$ Hz, 1H), 7.61 (s, 1H), 7.48 (d, $J = 15.3$ Hz, 1H), 7.43 (d, $J = 6.7$ Hz, 1H), 7.37 (t, 1H), 7.30 (d, $J = 6.9$ Hz, 1H), 3.58 (s, 1H), 3.03 (d, $J = 35.6$ Hz, 1H), 1.47 – 1.11 (m, 1H). HRMS (TOF-ESI, +ve): m/z ($\text{M}+\text{Na}^+$) Calcd for $\text{C}_{18}\text{H}_{16}\text{N}_2\text{O}_3\text{NaBrMn}$ 464.9622; Found 464.9644.

$[\text{MnBr}(\text{CO})_3(\text{DIPIMP})]$ (**3**)

$[\text{MnBr}(\text{CO})_5]$ (0.75 mmol, 0.2 g) was combined with DIPIMP (0.75 mmol, 0.2 g) in diethyl ether (20 ml) and refluxed under aerobic conditions for 4 h. The product was formed in 97% yield. $^1\text{H NMR}$ (500 MHz, CDCl_3) δ 9.30 (s, 1H), 8.41 (s, 1H), 7.99 (d, $J = 50.7$ Hz, 2H), 7.63 (s, 1H), 7.34 (s, 2H), 4.04 (s, 1H), 2.91 (s, 1H), 1.34 (d, $J = 3.1$ Hz, 6H), 1.05 (dd, $J = 80.6, 35.1$ Hz, 6H). HRMS (TOF-ESI, +ve): m/z ($\text{M}+\text{Na}^+$) Calcd for $\text{C}_{21}\text{H}_{22}\text{N}_2\text{O}_3\text{NaBrMn}$ 507.0092; Found 507.0107.

$[\text{MnBr}(\text{CO})_3(\text{TBIMP})]$ (**4**)

$[\text{MnBr}(\text{CO})_5]$ (0.84 mmol, 0.23 g) was combined with DIPIMP (0.84 mmol, 0.2 g) in diethyl ether (20 ml) and refluxed under aerobic conditions for 4 h. The product was formed in quantitative yield. $^1\text{H NMR}$ (400 MHz, CDCl_3) δ 9.27 (d, $J = 4.4$ Hz, 1H), 8.50 (s, 1H), 8.12 (d, $J = 6.9$ Hz, 1H), 8.03 (t, $J = 7.2$ Hz, 1H), 7.91 (d, $J = 7.1$ Hz, 1H), 7.61 (t, $J = 6.2$ Hz, 1H), 7.57 (d, $J = 7.4$ Hz, 1H), 7.30 (t, 1H), 1.43 (s, 1H). HRMS (TOF-ESI, +ve): m/z ($\text{M}+\text{Na}^+$) Calcd for $\text{C}_{19}\text{H}_{18}\text{N}_2\text{O}_3\text{NaBrMn}$ 478.9774; Found 478.9789.

$[\text{MnBr}(\text{CO})_3(\text{TBIEP})]$ (**5**)

$[\text{MnBr}(\text{CO})_5]$ (0.8 mmol, 0.22 g) was combined with TBIEP (0.8 mmol, 0.2 g) and refluxed under aerobic conditions in diethyl ether (20 ml) for 4 h. The product was formed in quantitative yield. $^1\text{H NMR}$ (400 MHz, CDCl_3) δ 9.28 (d, $J = 5.0$ Hz, 1H), 8.04 (td, $J = 7.8, 1.3$ Hz, 1H), 7.95 (d, $J = 7.7$ Hz, 1H), 7.88 (dd, $J = 6.1, 3.4$ Hz, 1H), 7.65 – 7.54 (m, 2H), 7.34 – 7.27 (m, 2H), 2.39 (s, 3H), 1.39 (s, 8H). HRMS (TOF-ESI, +ve): m/z ($\text{M}+\text{Na}^+$) Calcd for $\text{C}_{20}\text{H}_{20}\text{N}_2\text{O}_3\text{NaBrMn}$ 492.9935; Found 492.9934.

Complex $[\text{MnBr}(\text{CO})_3(\text{bpy})]$ (6**)** was prepared following literature procedure;² analytical data are in agreement with the literature data. $[\text{MnBr}(\text{CO})_5]$ (1.28 mmol, 0.35 g) was combined with 2,2'-bipyridine (1.28 mmol, 0.2 g) in diethyl ether (20 ml) and refluxed under aerobic conditions for 4 h. The product was formed in 80 % yield. $^1\text{H NMR}$ (500 MHz, CDCl_3) δ 9.27 (d, $J = 4.3$ Hz, 1H), 8.12 (d, $J = 6.5$ Hz, 1H), 7.99 (t, 1H), 7.53 (t, 1H). HRMS (TOF-ESI, +ve): m/z ($\text{M}+\text{Na}^+$) Calcd for $\text{C}_{13}\text{H}_8\text{N}_2\text{O}_3\text{NaBrMn}$ 396.8991; Found 369.8988.

Cyclic Voltammetry

Cyclic voltammetry was performed using a Princeton Applied Research VersaSTAT3 potentiostat on 2 mM **1-6** in Grubbs dried HPLC-grade acetonitrile containing 2×10^{-1} M $[\text{Bu}_4\text{N}][\text{PF}_6]$ as supporting electrolyte. A glassy carbon working electrode (surface area 0.07 cm^2 , polished on alumina and paper) and a Pt wire counter electrode were used with a 0.1 M KCl Ag/AgCl reference electrode.

The solutions were deoxygenated by bubbling thoroughly with bottled N_2 (BOC) and the N_2 atmosphere was maintained over the samples during the experiment. To test for catalytic current in presence of CO_2 , the samples were bubbled thoroughly with

bottled CO₂ (BOC) and cyclic voltammograms (CVs) were recorded under the atmosphere of CO₂ (some residual water might be present in the CO₂ used to saturate the samples). Water was then added (0.3 ml to 6 ml of the solution of each sample) to test the effects of Brønsted acid. Ferrocene was added as the internal standard at the end of all experiments.

Spectroelectrochemistry

Infrared spectroelectrochemistry was performed using an EmStat3 or EmStat3+ potentiostat (PalmSense, The Netherlands). The solution of 4 mM complex in the presence of 3×10^{-1} M [Bu₄N][PF₆] in dry acetonitrile was analyzed using an optically transparent thin-layer electrochemical (OTTLE) cell equipped with Pt minigrad working and auxiliary electrodes, an Ag microwire pseudoreference electrode and CaF₂ windows. Samples were prepared under an argon atmosphere; for electrocatalytic measurements, the solutions were bubbled with CO₂ on a frit (a few minutes) to saturation under normal pressure. Parallel IR and UV-vis spectral monitoring during the spectroelectrochemical experiment was performed on a Bruker Vertex 70v FT-IR spectrometer or Perkin Elmer Spectrum 1, and a Scinco S-3100 spectrophotometer, respectively. Thin-layer CVs were recorded in the course of the experiment.

Gas Chromatography Linked to Electrolysis

Bulk electrolysis was performed on a 0.17 mM solution of each of the complexes in a 60 ml solution of acetonitrile/water (9:1 v/v). The cell set up consisted of a Pt mesh working electrode, a Pt rod counter-electrode in a semi-porous compartment, and an Ag wire pseudo-reference electrode in a 0.1 M KCl solution. The potential of the Fc/Fc⁺ recorded in this set-up using glassy-carbon 3-mm diameter electrode was +0.350 vs. Ag wire pseudo-reference. Hence in order to reach the potential necessary for the CO₂ reduction as estimated from the CV data, the potential was held at -1.9 V vs Ag wire for all samples, i.e., -2.25V vs. Fc/Fc⁺. Prior to electrolysis, a CV was recorded in the bulk electrolysis cell using glassy-carbon working electrode. 100 μl gas samples were withdrawn from the head space at regular intervals and analysed by a gas chromatograph fitted with a thermal conductivity detector; Perkin ElmerArnel autosystem XL. H₂ was used as the carrier gas in CO-quantification experiments. N₂ was used as a carrier gas in the control experiment.

X-ray Crystallography

Crystals were grown using anti-solvent crystallization method, with the solvent dichloromethane and hexane as the anti-solvent. Single-crystal X-ray diffraction data were collected on a Bruker SMART APEX-II CCD diffractometer operating a Mo-K_α sealed-tube X-ray source or a Bruker D8 Venture diffractometer equipped with a PHOTON 100 dual-CMOS chip detector and operating a Cu-K_α I μ S microfocus X-ray source. The data were processed using Bruker APEX3 software and corrected for absorption using empirical methods (SADABS) based upon symmetry-equivalent reflections combined with measurements at different azimuthal angles.⁴⁰ The crystal structures were solved and refined using the Bruker SHELXTL software package.

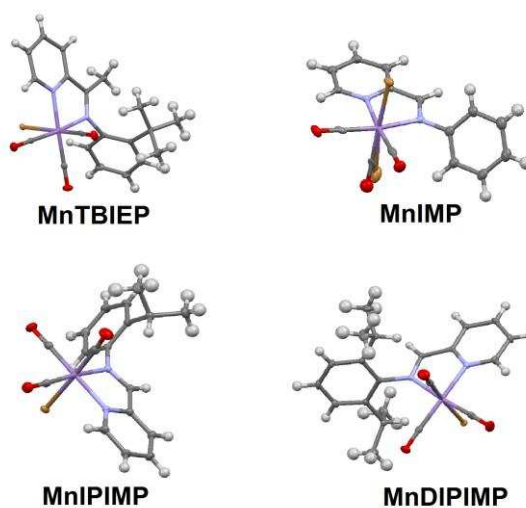


Figure 1. X-ray crystal structures of the studied complexes shown with thermal ellipsoids at the 50 % probability level. CCDC 1457930, MnTBIEP, 1457931, MnDIPIMP, 1457932, MnIPIMP, 1457933, MnIMP. Full crystallographic details are given in the Supporting Information.

Computational Methods

Density functional theory (DFT) calculations were performed using the Gaussian 09 program package.⁴¹ All calculations utilised the global hybrid exchange correlation functional B3LYP,^{42,43} a ‘mixed’ basis set consisting of the SDD basis set as defined in Gaussian for Mn and the 6-311G(d,p) basis set for all other atoms.^{44,45,46,47} The solvent acetonitrile was included using the Polarizable Continuum Model (PCM) as implemented in Gaussian.^{48,49} All species were modelled at the lowest multiplicity appropriate for the electron count and the restricted formalism was used for closed shell cases. An ‘ultrafine’ integral grid, as defined by Gaussian, was used and all geometries were confirmed as minima by the absence of imaginary frequencies in their vibrational spectra as calculated within the harmonic approximation. The values of vibrational frequencies have been scaled by 0.966 to match experimental $\nu(\text{CO})$ of the parent neutral complexes.

Results and Discussion

X-ray Crystallography

The crystal structures of the complexes [MnBr(CO)₃(α -diimine)] (α -diimine = TBIEP, IMP, IPIMP, DIPIMP) are shown in Figure 1, and selected bond distances and angles are listed in Supporting Information, Table SI 1. Similar bond lengths are observed for the four complexes, and these are in good agreement with related [MnBr(CO)₃(α -diimine)] species reported in the literature. The X-ray data are in good agreement with the results obtained through DFT calculations. As predicted by DFT, the pyridine and phenyl rings lie approximately orthogonally to one another (dihedral angles between the corresponding planes are: MnTBIEP, 84.55°; MnIPIMP, 83.64°, MnDIPIMP, 78°), resulting in little orbital overlap between these two moieties, with the exception of MnIMP where the two ring systems were significantly less orthogonal (56.54°).

The crystal structures have revealed significant steric hindrance between the substituents R = Me and the R₁ = ^tBu in MnTBIEP, which inhibits rotation of the Ph-ring and confers conformational rigidity. Rotation of the Ph-ring in MnDIPIMP is also inhibited by the two ⁱPr groups and hence also has the conformational rigidity. In contrast, MnIMP and MnIPIMP exhibit much smaller steric hindrance, facilitating the rotation of the phenyl ring.

Computational Investigations of Molecular Structures and Frontier Orbitals by DFT

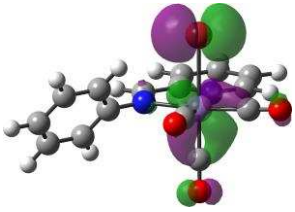
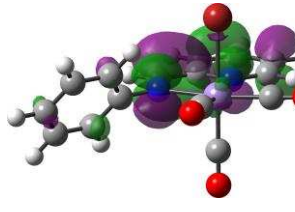
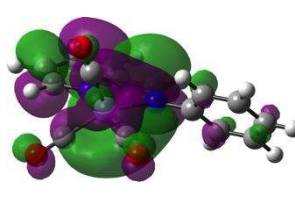
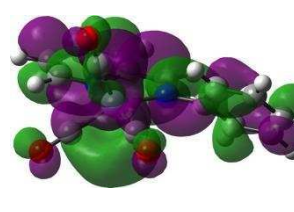
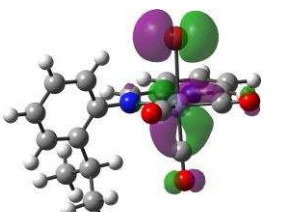
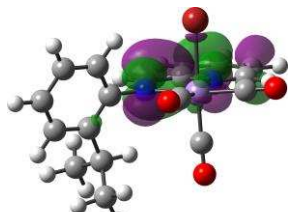
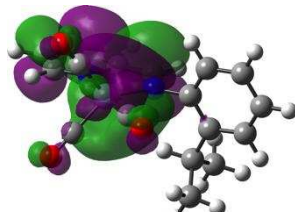
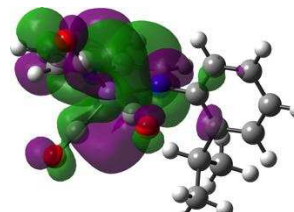
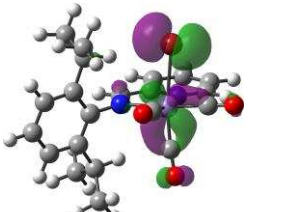
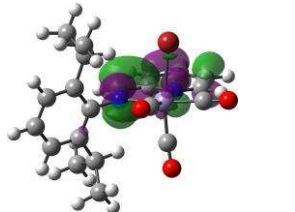
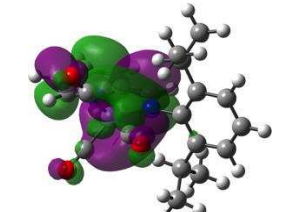
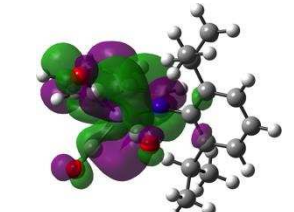
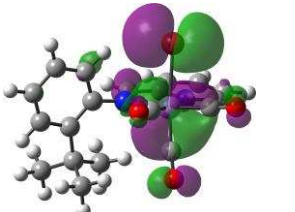
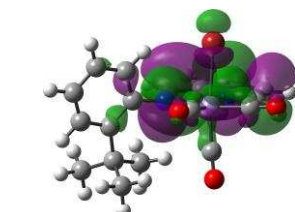
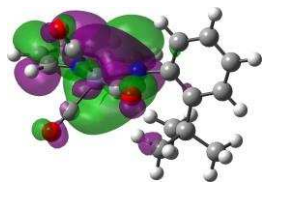
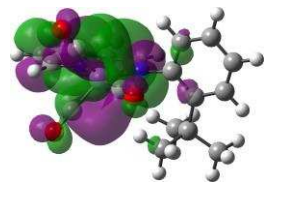
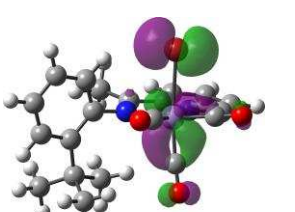
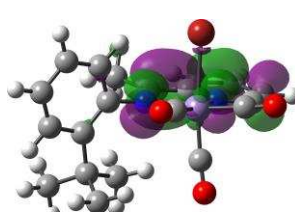
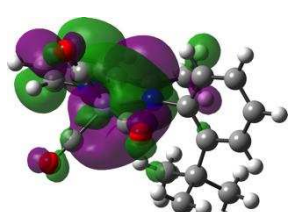
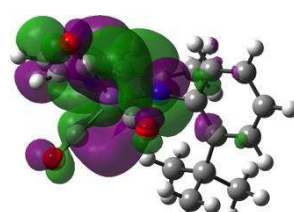
The optimized geometries of the studied complexes with frontier orbitals overlaid as calculated by DFT are displayed in Table 2. As anticipated, the phenyl group lies out of plane of the chelating diimine. The HOMO is localized predominantly over the axial Br–Mn–C(O) bonds with almost no contribution from the phenyl moiety. The LUMO resides largely on the imine, pyridyl and metal center, with minimal contribution from the C1–C2 and C1–C6 σ bonds of the phenyl groups. In the case of MnIMP, due to the lack of substitution at R₁ and R₂, the phenyl moiety is less sterically hindered and thus is positioned closer to the plane of the imino-pyridine fragment, resulting in a small degree of involvement of the phenyl π -system in the low energy unoccupied orbitals. This trend continues in the other low-energy unoccupied orbitals (see Supporting Information, Figures SI 1-10).

Table 1. Experimentally obtained and calculated frequencies of carbonyl stretching vibrations, $\nu(\text{CO})$, of the Mn complexes in their neutral form (**1-5**), transient one-electron reduced form, as well as 5-coordinate anion, a cationic aqua complex, and an Mn–Mn bound dimer, in acetonitrile at 293 K.

Species	$\nu(\text{CO}) / \text{cm}^{-1}$	$\nu(\text{CO}) / \text{cm}^{-1}$
	Calculated	Experimental
[MnBr(CO) ₃ (IMP)] (1)	2020, 1943, 1931	2029, 1941, 1926
[MnBr(CO) ₃ (IMP)] [−]	1992, 1906, 1897	Not observed
[Mn(CO) ₃ (H ₂ O)(IMP)] ⁺	2046, 1966, 1957	2051, 1964 ^b , 1958 ^t
[Mn(CO) ₃ (IMP)] [−]	1906, 1830, 1813	1930, 1826
[Mn(CO) ₃ (IMP)] ₂	1964, 1918, 1891, 1882, 1872, 1868	1994, 1949, 1902, 1875
[MnBr(CO) ₃ (IPIMP)] (2)	2020, 1945, 1929	2029, 1943, 1923
[MnBr(CO) ₃ (IPIMP)] [−]	1988, 1905, 1891	Not observed
[Mn(CO) ₃ (H ₂ O)(IPIMP)] ⁺	2044, 1963, 1956	2049, 1959(br)
[Mn(CO) ₃ (IPIMP)] [−]	1905, 1826, 1808	1929, 1824
[Mn(CO) ₃ (IPIMP)] ₂	1964, 1917, 1890, 1881, 1866, 1860	1981, 1949, 1901, 1882, 1862
[MnBr(CO) ₃ (DIPIMP)] (3)	2019, 1945, 1929	2028, 1944, 1922
[MnBr(CO) ₃ (DIPIMP)] [−]	1985, 1906, 1890	Not observed
[Mn(CO) ₃ (H ₂ O)(DIPIMP)] ⁺	2045, 1964, 1957	2050, 1960(br) ^b
[Mn(CO) ₃ (DIPIMP)] [−]	1903, 1824, 1806	1929, 1829/22
[Mn(CO) ₃ (DIPIMP)] ₂	1965, 1918, 1890, 1880, 1860, 1850	Not observed
[MnBr(CO) ₃ (TBIMP)] (4)	2020, 1947, 1925	2029, 1945, 1923
[MnBr(CO) ₃ (TBIMP)] [−]	1988, 1907, 1890	Not observed
[Mn(CO) ₃ (H ₂ O)(TBIMP)] ⁺	2045, 1965, 1956	Not observed
[Mn(CO) ₃ (TBIMP)] [−]	1906, 1827, 1807	1928, 1823
[Mn(CO) ₃ (TBIMP)] ₂	1964, 1916, 1889, 1879, 1862, 1854	Not observed
[MnBr(CO) ₃ (TBIEP)] (5)	2018, 1944, 1921	2028, 1943, 1917
[MnBr(CO) ₃ (TBIEP)] [−]	1980, 1904, 1883	Not observed
[Mn(CO) ₃ (H ₂ O)(TBIEP)] ⁺	2042, 1962, 1950	2048, 1960, 1954
[Mn(CO) ₃ (TBIEP)] [−]	1897, 1819, 1798	1922, 1814(br)
[Mn(CO) ₃ (TBIEP)] ₂	1958, 1909, 1880, 1870, 1850, 1841	Not observed

^a In acetonitrile at 293 K. ^b Positions are approximate as the parent CO stretching vibrations obscure those of the cationic aqua complex.

Table 2. Frontier orbitals of the complexes 1-5 and the corresponding 5-coordinate anions calculated at the B3LYP/SDD+6-311G(d,p)/IEFPCM level. Isovalue of $0.04 \sqrt{e^- \text{ bohr}^{-3}}$.

HOMO	LUMO	HOMO	LUMO
Parent Complex		Five-coordinate anion	
MnIMP		MnIMP	
			
$\epsilon = -6.31 \text{ eV}$	$\epsilon = -2.84 \text{ eV}$	$\epsilon = -3.67 \text{ eV}$	$\epsilon = -1.18 \text{ eV}$
MnIPIMP		MnIPIMP	
			
$\epsilon = -6.33 \text{ eV}$	$\epsilon = -2.81 \text{ eV}$	$\epsilon = -3.70 \text{ eV}$	$\epsilon = -1.01 \text{ eV}$
MnDIPIMP		MnDIPIMP	
			
$\epsilon = -6.31 \text{ eV}$	$\epsilon = -2.83 \text{ eV}$	$\epsilon = -3.67 \text{ eV}$	$\epsilon = -0.99 \text{ eV}$
MnTBIMP		MnTBIMP	
			
$\epsilon = -6.36 \text{ eV}$	$\epsilon = -2.80 \text{ eV}$	$\epsilon = -3.64 \text{ eV}$	$\epsilon = -1.02 \text{ eV}$
MnTBIEP		MnTBIEP	
			
$\epsilon = -6.33 \text{ eV}$	$\epsilon = -2.62 \text{ eV}$	$\epsilon = -3.55 \text{ eV}$	$\epsilon = -0.99 \text{ eV}$

The energies of the HOMO in all complexes are within 0.02 eV of each other and all the IMP subset of complexes have a LUMO that lie within 0.03 eV of the other complexes. In contrast MnTBIEP shows a difference in LUMO energy of +0.19 eV compared with IPIMP. This larger difference in LUMO energy comes as result of methylation at the R position. In contrast, adding two isopropyl groups at the R₁ and R₂ positions resulted in an energy difference of just 0.02 eV between MnIMP and MnDIPIMP. The results of the calculations on the trends in the energies of HOMO/LUMO are in full agreement with the experimentally determined redox potentials (see below). These results imply that an almost complete separation between the steric and the electronic effects in the context of few-electron reductions can indeed be achieved in this series of complexes. Changing the R group will strongly affect the energy of the LUMO while having also some impact on the steric properties at the carbon of imino C=N bond, whilst changing the R₁ or R₂ groups should have considerable effects on the steric hindrance of the molecule (protecting the Mn and imino-N centers), but hardly affecting its electronic properties.

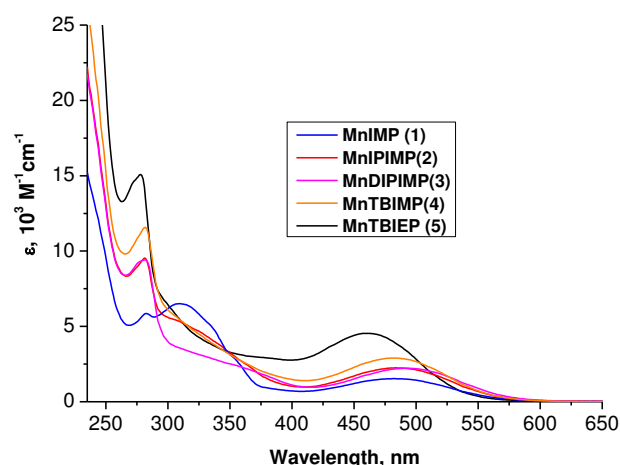


Figure 2. Electronic absorption spectra of the manganese complexes **1-5** studied in this work, in DCM at 293 K.

The experimental and calculated carbonyl vibrational frequencies of the studied complexes are shown in Table 1. The calculated frequencies are in good agreement with the experimental values. Some systematic discrepancies are apparent: the high energy A'(1) mode tends to be underestimated by ~ 10 cm^{-1} , the A'' mode tends to have a lower deviation of only ~ 2 cm^{-1} , and the low energy A'(2) mode tends to be overestimated by ~ 10 cm^{-1} . It is clear that attachment of the methyl group as R increases the electron density on the metal center and thus also the Mn-to-CO π -back bonding, as evidenced by the smaller values of $\nu(\text{CO})$ for MnTBIEP compared to the IMP sub-series (complexes **1-4**). However, substitution at R₁ and R₂ has only little effect on the frequencies. It should be noted that the magnitude of these effects is small (<10 cm^{-1}) and that it is beyond the scope of this computational work to unravel the various factors effecting changes in CO stretching frequencies.⁵⁰

The results of DFT calculations (Table 1) of IR spectra for the parent Br-complexes, $[\text{MnBr}(\text{CO})_3(\alpha\text{-diimine})]$ **1-5**, and the corresponding $[\text{Mn}(\text{CO})_3(\text{H}_2\text{O})(\alpha\text{-diimine})]^+$ (cationic aquo complexes) match well the experimental data. We therefore

use the calculated $\nu(\text{CO})$ wavenumbers for the hydrolysed aquo and reduced (dimer and anion) species to aid the analysis of the IR spectra and product assignment in the course of the corresponding cathodic IR-SEC experiments (vide infra).

Adding electron-donating groups (ⁱPr, ^tBu) to the phenyl ring of the IMP subseries does not have a large effect on the $\nu(\text{CO})$ frequency, the band positions being virtually unchanged between complexes **1-4**. The two higher-frequency bands are at 2028-2029 cm^{-1} and 1943-1944 cm^{-1} for all 5 complexes, whilst the lowest $\nu(\text{CO})$ band is seen at 1923-1922 cm^{-1} for the "IMP" series but shifted to lower energy, 1917 cm^{-1} in $[\text{MnBr}(\text{CO})_3(\text{TBIEP})]$ where the increased π -back-donation is caused by R = Me. This invariability of $\nu(\text{CO})$ frequencies, whilst the dihedral angle between the planes of the pyridine and phenyl moieties of the IP ligands is clearly changing drastically, from ~ 56 to $\sim 84^\circ$, confirm the opportunity of the somewhat independent tuning of electronic and steric factors.

Calculations performed on the five-coordinate anions of the studied compounds, $[\text{Mn}(\text{CO})_3(\text{diimine})]^-$, show very similar trends to what has been observed in the parent complexes. Both the HOMO and LUMO are predominantly delocalized over the tricarbonyl-Mn and α -diimine metalacycle, with little participation from the phenyl ring, with the exception of MnIMP, the LUMO of which having a significant contribution from the phenyl moiety.

The UV-vis absorption spectra (Figure 2) are consistent with the nature of the frontier orbitals obtained from the calculated data. The lowest energy absorption band for the complexes of the IMP sub-series **1-4**, occurs at approximately the same, ca. 500-nm position. In contrast MnTBIEP (**5**) exhibits an absorption band with maximum at a shorter wavelength, 460 nm, due to electron donation from the Me group which destabilizes the LUMO.

Cyclic Voltammetry

Electrochemical studies showed significant differences between the cathodic path of MnTBIEP (**5**) and those of the IMP sub-series (**1-4**).

Under an N₂ atmosphere, $[\text{MnBr}(\text{CO})_3(\text{TBIEP})]$ shows a single reduction wave at $E_{p,c}$ -1.53 V and an intense anodic wave at $E_{p,a}$ = -1.3 V observed on the reverse anodic scan.

This behavior is similar to that of $[\text{MnBr}(\text{CO})_3(^i\text{Pr-DAB})]$ (ⁱPr-DAB: 1,4-diisopropyl-1,4-diazabuta-1,3-diene),⁸ which is reduced by an ECE mechanism. The initial one-electron reduction results in dissociation of the bromide to form a five-coordinate radical, $[\text{Mn}(\text{CO})_3(\text{TBIEP})]^\cdot$, which is concomitantly reduced to the five-coordinate anion $[\text{Mn}(\text{CO})_3(\text{TBIEP})]^-$ (re-oxidized at -1.3 V) at the potential required for the reduction of $[\text{MnBr}(\text{CO})_3(\text{TBIEP})]$. A small anodic wave at -0.6 V is characteristic of oxidation of $[\text{Mn}(\text{CO})_3(\text{TBIEP})]_2$ formed in the course of the anodic path of the five-coordinate anion, and indicates that dimerization can still occur with the R = CH₃. The dimer could also be produced in a reaction of $[\text{Mn}(\text{CO})_3(\text{TBIEP})]^-$ with neutral $[\text{MnBr}(\text{CO})_3(\text{TBIEP})]$ on the cathodic scan; but the absence of a cathodic wave for reduction of $[\text{Mn}(\text{CO})_3(\text{TBIEP})]_2$ indicates that its reduction poten-

tial is too close to that of $[\text{MnBr}(\text{CO})_3(\text{TBIEP})]$ for a separate reduction wave to be observed.

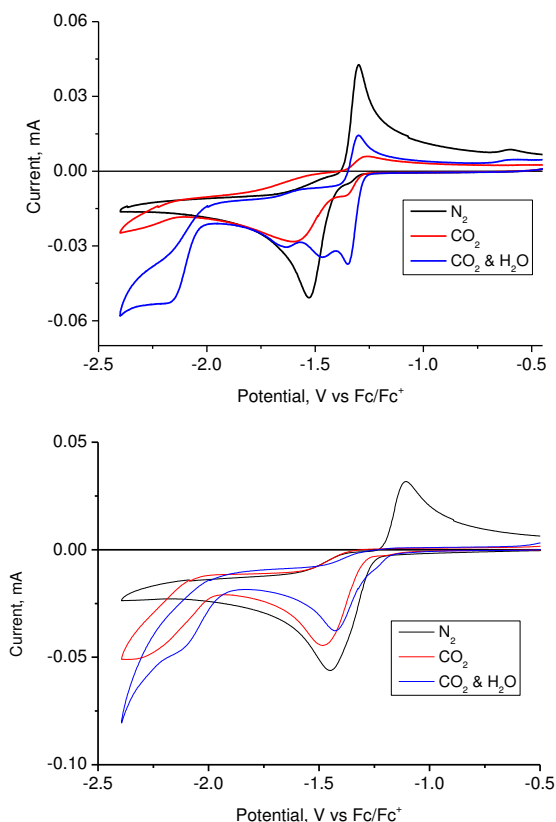


Figure 3. Cyclic voltammograms of 1 mM MnTBIEP (top panel) and MnTBIMP (bottom panel) in acetonitrile, 0.2 M $[\text{Bu}_4\text{N}][\text{PF}_6]$ as supporting electrolyte, under N_2 atmosphere (black), CO_2 atmosphere (red) and CO_2 with 4.7% added water (blue) at scan rate 0.1 V s^{-1} .

The CV traces of MnIMP obtained under N_2 atmosphere show three cathodic reduction peaks, at $E_{p,c} = -1.28, -1.41$ and -1.54 V and a strong anodic peak at $E_{p,a} = -1.24 \text{ V}$. The first reduction at -1.28 V can be assigned to the cation $[\text{Mn}(\text{CO})_3(\text{H}_2\text{O})(\text{IMP})]^+$; it is likely that the peak at -1.41 V is due to remaining non-hydrolyzed $[\text{MnBr}(\text{CO})_3(\text{IMP})]'$ or a solvent adduct,¹¹ whilst the -1.54 V wave corresponds to the reduction of the dimeric species (see also the IR spectroelectrochemical section below). The 5-coordinate anion $[\text{Mn}(\text{CO})_3(\text{IMP})]^-$ is probably the reduction product at all three different cathodic waves (the parent complex $[\text{MnBr}(\text{CO})_3(\text{IMP})]$, aquo-complex, and the IMPMn–MnIMP dimer), as evidenced by its anodic wave at $E_{p,a} = -1.24 \text{ V}$ on the reverse anodic scan (accompanied by the dimer oxidation above -0.5 V).

Over time a smaller cathodic wave emerges at $E_{p,c} -1.35 \text{ V}$, due to the aquo-coordinated cationic complex forming via hydrolysis of the parent Br-complex (see Supporting Information, Figure SII1-SII2). Under an atmosphere of CO_2 the anodic wave of $[\text{Mn}(\text{CO})_3(\text{TBIEP})]^-$ at -1.3 V disappears, and the profile of the CV also changes, (Figure 3), with a broad cathodic wave of $[\text{MnBr}(\text{CO})_3(\text{TBIEP})]$ shifted slightly negatively, indicating an interaction with CO_2 . However, similar to Mn–bpy complexes,² catalytic reduction of CO_2 in the absence

of a Brønsted acid was not observed (the small peak beginning around -2.18 V is due to a small amount of water entering the CV cell when it is being saturated with CO_2). Addition of 0.3 ml of water leads to significant current enhancement at -2.18 V in line with what has been observed with $[\text{MnBr}(\text{CO})_3(\text{iPr-DAB})]$.⁸

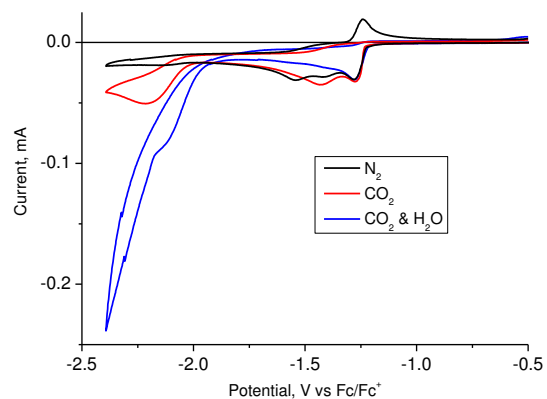


Figure 4. Cyclic voltammograms of 1 mM MnIMP in acetonitrile, 0.2 M $[\text{Bu}_4\text{N}][\text{PF}_6]$, scan rate 0.1 V s^{-1} . Under atmosphere of N_2 (black), CO_2 (red), and CO_2 with 4.7% H_2O (blue).

Under CO_2 atmosphere, the increased cathodic current is seen at $\sim -2.2 \text{ V}$ for all complexes. We believe this is due to some amount of the bicarbonate complex being formed, likely due to traces of water in the CO_2 used.³³ When 10% water is added to the CO_2 saturated solution, a strong current enhancement is observed at -2.21 V . Importantly, CVs recorded under N_2 atmosphere in acetonitrile in presence of water do not show catalytic current enhancement (see Supplementary Figures SII4-SII8); thus, both CO_2 and water are required for the current enhancement to be observed.

Under CO_2 atmosphere, no anodic wave corresponding to re-oxidation of the five-coordinate anion is observed for the least sterically hindered $[\text{Mn}(\text{CO})_3(\text{IMP})]^-$ (Fig. 4), and for the monosubstituted complexes **2** and **4**; a behavior indicative of a rapid reaction of the anion with CO_2 . A diminished but clear anodic wave of $[\text{Mn}(\text{CO})_3(\text{TBIEP})]^-$ can be observed under CO_2 vs. N_2 atmosphere (Figure 3), suggesting that $[\text{Mn}(\text{CO})_3(\text{TBIEP})]^-$ associates with CO_2 less efficiently. Whilst, similarly to MnIPIMP, no anodic wave corresponding to $[\text{Mn}(\text{CO})_3(\text{TBIMP})]^-$ re-oxidation under CO_2 atmosphere could be observed indicating that CO_2 association is rapid, the overall current enhancement for this complex is comparatively low indicating lower efficiency at reducing CO_2 , perhaps due to the bicarbonate intermediate somewhat preventing the recovery of the 5-coordinate catalytic species.

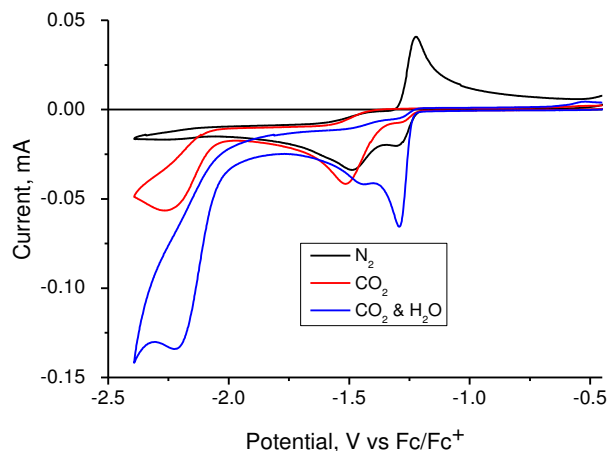


Figure 5. Cyclic voltammograms of 1 mM MnIPIMP in acetonitrile, 0.2M [Bu₄N][PF₆], scan rate 0.1 V s⁻¹. Under atmosphere of N₂ (black), CO₂ (red), and CO₂ with 4.7% H₂O (blue).

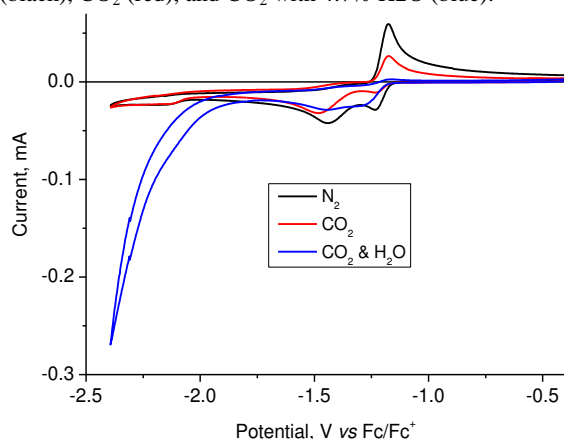


Figure 6. Cyclic voltammograms of 1 mM MnDIPIMP in acetonitrile, 0.2M [Bu₄N][PF₆], scan rate 0.1 V s⁻¹. Under atmosphere of N₂ (black), CO₂ (red), and CO₂ with 4.7% H₂O (blue).

Under N₂, reduction of [MnBr(CO)₃(IPIMP)] is seen at E_{p,c} -1.49 V, accompanied by a wave at E_{p,c} -1.29 V, assigned to the cationic aqua complex [Mn(CO)₃(H₂O)(IPIMP)]⁺. As discussed above, upon addition of CO₂ the oxidation wave of the anion [Mn(CO)₃(IPIMP)]⁻ is not observed, indicating a rapid reaction between the 5-coordinate anion and CO₂. Some current enhancement at -2.26 V is observed upon saturation with CO₂ which is enhanced greatly upon the addition of 0.3 ml of water (the current enhancement corresponds to the cathodic wave of the bicarbonate complex, identified in the IR spectra (vide infra): some catalysis occurs due to hydrolysis caused for example by residual water in the electrolyte, or in the CO₂).

CV of MnTBIMP (Figure 3, bottom panel) is similar to that of MnIPIMP and MnTBIEP with a strong cathodic wave at -1.45 V. At ca. -2.28 V current enhancements ascribed to CO₂ reduction can be observed under CO₂ and CO₂ with added H₂O, though the i_{cat}/i_p values (Table SI1) are somewhat lower compared to the other complexes studied here. Importantly, the anodic wave of the five-coordinate anion re-oxidation is not detected for MnIPIMP and MnTBIMP, but is clearly seen for slower reacting MnTBIEP and MnDIPIMP anions.

MnDIPIMP shows significant differences in the CV traces to the other complexes of the IMP sub-series. Similarly to the IMP and IPIMP complexes, a formation of an aqua-cation complex ([Mn(CO)₃(H₂O)(DIPIMP)]⁺) is observed in solution. However, upon saturation with CO₂ no additional processes (intermediate bicarbonate complex reduction) or current enhancement below -2 V are observed and the anodic peak due to oxidation of [Mn(CO)₃(DIPIMP)]⁻ does not fully disappear. This suggests that the reduced complex is less prone to interact with CO₂, as would be expected due to the increased steric hindrance and structural rigidity of the complex arising from the two ⁱPr- substituents at the N-phenyl rings.

Table 3. Cathodic potentials (V, vs. Fc/Fc⁺) of the parent complexes [MnBr(CO)₃(IP)] (1 mM, acetonitrile, 0.2 M [Bu₄N][PF₆]) and corresponding cationic Mn-aquo derivatives formed in situ by partial hydrolysis

Complex	E _{p,c}	Catalytic potential ^b
[MnBr(CO) ₃ (IMP)] (1)	-1.41, -1.54 ^a	-2.21
[Mn(CO) ₃ (H ₂ O)(IMP)] ⁺	-1.28	
[MnBr(CO) ₃ (IPIMP)] (2)	-1.49	-2.26
[Mn(CO) ₃ (H ₂ O)(IPIMP)] ⁺	-1.29	
[MnBr(CO) ₃ (DIPIMP)] (3)	-1.44	-2.16
[Mn(CO) ₃ (H ₂ O)(DIPIMP)] ⁺	-1.23	
[MnBr(CO) ₃ (TBIMP)] (4)	-1.45	~ -2.28
[MnBr(CO) ₃ (TBIEP)] (5)	-1.53	-2.18
[Mn(CO) ₃ (H ₂ O)(TBIEP)] ⁺	-1.35	

^aThis process probably corresponds to a reduction of the dimer; ^bLargely coinciding with the reduction of a bicarbonate complex (see the spectroelectrochemical section).

IR and UV-vis Spectroelectrochemistry under Inert Atmosphere

IR spectroscopy^{20,53,54} is an ideal tool to monitor the cathodic processes in the studied complexes, due to presence of the carbonyl ligands as strong IR reporters. Table 1 lists the key experimental and calculated vibrational frequencies for the starting complexes and several relevant intermediate and dimer species. IR spectroelectrochemistry (IR-SEC) was used to probe the intermediates produced upon reduction and to monitor their presence during CO₂ reduction.

IR spectra of MnTBIEP (Figure 7) show, upon the first reduction, depletion of the parent ν(CO) bands, with new bands growing in at 1922 cm⁻¹, 1898 cm⁻¹ and a broad feature at 1814 cm⁻¹. The bands at 1922 cm⁻¹ and 1814 cm⁻¹ can be assigned to the five-coordinate anion [Mn(CO)₃(TBIEP)]⁻, an assignment supported by DFT calculations. The band at 1898 cm⁻¹, which grows in after the five-coordinate anion begins to form, could tentatively be attributed to a decomposition product. UV/Vis spectro-electrochemistry (Supporting Information, Figure SI 13) supports this notion as only a band at ca. 570 nm has been detected, which corresponds to the five-coordinate anion. Differently from the MnIMP and MnIPIMP complexes (see below), there is no indication of a dimer ([Mn(CO)₃(TBIEP)]₂) formation during the reduction of MnTBIEP on the timescale of the experiments performed.

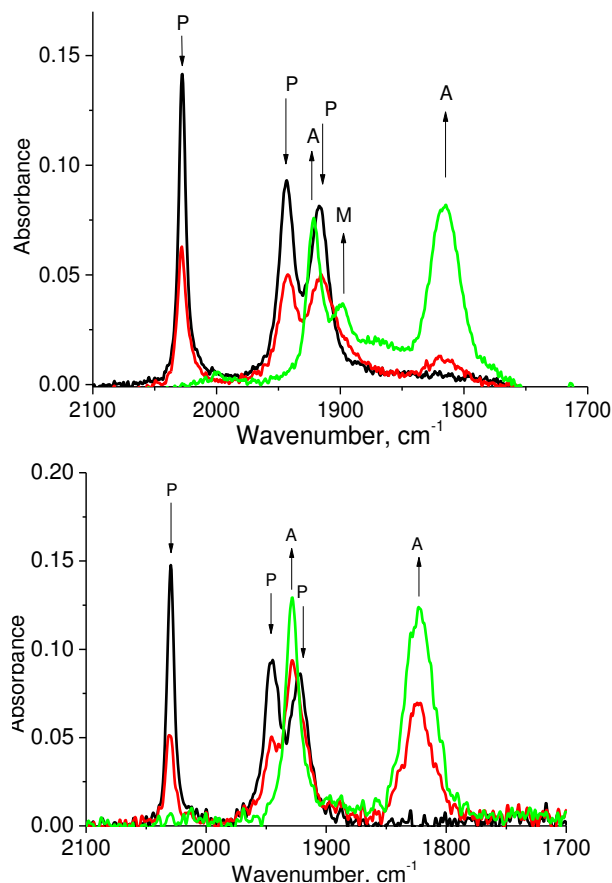


Figure 7. IR spectral changes accompanying in situ reduction of complexes in Ar-saturated acetonitrile/0.2 M $[\text{Bu}_4\text{N}][\text{PF}_6]$ within an OTTLE cell. Top panel: For MnTBIEP, A direct reduction of the parent complex (black line) to 5-coordinate anion (green line) is observed. (P) $[\text{MnBr}(\text{CO})_3(\text{TBIEP})]$; (A) $[\text{Mn}(\text{CO})_3(\text{TBIEP})]^-$; (M) an unassigned side product. Bottom panel: For MnTBIMP, A direct reduction of the parent complex (black line) to 5-coordinate anion (green line) is observed. (P) $[\text{MnBr}(\text{CO})_3(\text{TBIMP})]$; (A) $[\text{Mn}(\text{CO})_3(\text{TBIMP})]^-$.

MnTBIMP mirrors the behavior of MnTBIEP with the bands at 2029, 1945 and 1923 cm^{-1} corresponding to the parent complex being replaced concertedly with bands at 1928 and 1823 cm^{-1} corresponding to the five-coordinate anion, with no intermediate species being observed. This would suggest that the direct formation of the five-coordinate anion is due to the steric demands of the ^tBu group, since the mono-ⁱPr derivative **2** does exhibit dimer formation (Table 1).

The results of the IR-SEC study of MnIMP are shown in Fig. 8. The first reduction of MnIMP in CH_3CN under an Ar atmosphere is accompanied by depletion of the parent IR bands at 2029, 1941 and 1926 cm^{-1} . Simultaneously, it shows the growth of new bands at 1994, 1949, 1902 and 1875 cm^{-1} , which are characteristic of the Mn–Mn dimer^{8,9,13,30} $[\text{Mn}(\text{CO})_3(\text{IMP})]_2$. Additionally, a peak at 2051 cm^{-1} grows in initially, which is assigned to the intermediate aqua-cation $[\text{Mn}(\text{CO})_3(\text{H}_2\text{O})(\text{IMP})]^+$ observed also by cyclic voltammetry. Further reduction of the dimer leads to formation of broad absorption bands at 1826 cm^{-1} and 1930 cm^{-1} , once the formation of the dimer species is complete. These features are

characteristic of the formation of the five-coordinate anion,^{8,9,13} $[\text{Mn}(\text{CO})_3(\text{IMP})]^-$. UV-Vis spectroelectrochemistry performed in parallel with the IR-SEC experiment confirms the presence of both of these species (Supporting Information, Figure SI14) via the broad absorption band at ca. 800 nm (assigned to the dimer) and the intense absorption at ca. 675 nm (assigned to the five-coordinate anion).⁸ All complexes in the IMP subseries exhibited a small transient peak at ca. 2050 cm^{-1} upon reduction. This is assigned to the aquo-complex $[\text{Mn}(\text{CO})_3(\text{H}_2\text{O})(\text{IMP})]^+$.

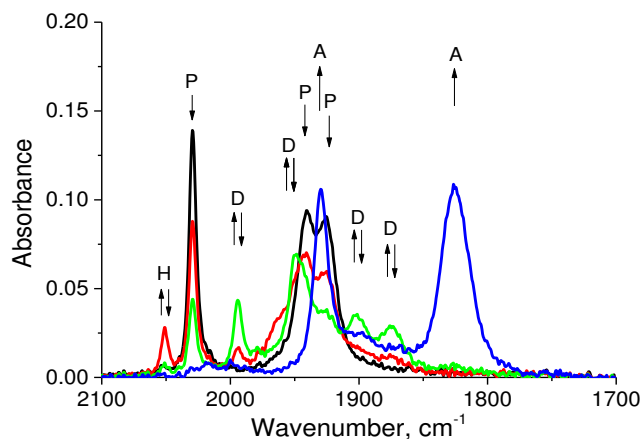


Figure 8. IR spectral changes accompanying in-situ reduction of MnIMP in Ar-saturated acetonitrile / 0.2 M $[\text{Bu}_4\text{N}][\text{PF}_6]$ within an OTTLE cell. The parent complex $[\text{MnBr}(\text{CO})_3(\text{IMP})]$ (**P**, black line), and aquo-cation $[\text{Mn}(\text{CO})_3(\text{H}_2\text{O})(\text{IMP})]^+$ (**H**, additional features in the red spectrum) are reduced to a dimer $[\text{MnBr}(\text{CO})_3(\text{IMP})]_2$ (**D**, green line) followed by reduction of the dimer to 5-coordinate anion $[\text{Mn}(\text{CO})_3(\text{IMP})]^-$ (**A**, blue line). The intermediate spectrum (red line) recorded between those of the parent complex and the dimer also shows the features of the aquo-complex.

Differently to MnIMP, MnIPIMP showed concurrent formation of the dimer and the five-coordinate anion upon reduction of the parent complex (Figure 9, top). The introduction of the isopropyl substituent at the phenyl ring leads to the observation of a small amount of five-coordinate anion $[\text{Mn}(\text{CO})_3(\text{IPIMP})]^-$ (absorbing at 1929 cm^{-1} and 1824 cm^{-1}), which grows in alongside peaks indicative of dimer formation (1981, 1949, 1901, 1882 and 1862 cm^{-1}).

Importantly, the IR absorption bands, corresponding to both the dimer and the five-coordinate anion, grew in simultaneously. UV-Vis spectroelectrochemistry confirmed the presence of both dimer and five-coordinate species in this case, as is evident from Figure SI13 (Supporting Information).

In contrast, only the five-coordinate anion detected already from the onset of the reduction of MnDIPIMP under the experimental conditions used. In this case, there is no evidence for the dimer formation during the reduction of parent complex. As shown in Figure 9 (bottom), an intense peak at 1823 cm^{-1} , assigned to the five-coordinate anion, grew in, followed closely by smaller peaks at 2007 cm^{-1} , and 1899 cm^{-1} . The second peak assigned to the five-coordinate anion at 1929 cm^{-1}

was masked by the absorption of the parent complex at the beginning of the reduction process. We tentatively assign the peaks at 2007 cm^{-1} / 1899 cm^{-1} to a solvent coordinated radical species $[\text{Mn}(\text{CO})_3(\text{MeCN})(\text{DIPIMP})]^*$, on the analogy with $[\text{Re}(\text{CO})_3(\text{PrCN})(^i\text{Pr-PyCa})]^{17}$ ($^i\text{Pr-PyCa}$ = iso-propyl-imino-pyridine; PrCN = butyronitrile) which shows $\nu(\text{CO})$ at 2005 cm^{-1} and $1885(\text{br})\text{ cm}^{-1}$. Further, since the anodic wave of the dimer oxidation is not observed in the CV of MnDIPIMP, but a 1e reduced radical species are observed in IR-SEC, it is evident that the DIPIMP ligand prevents dimerization.

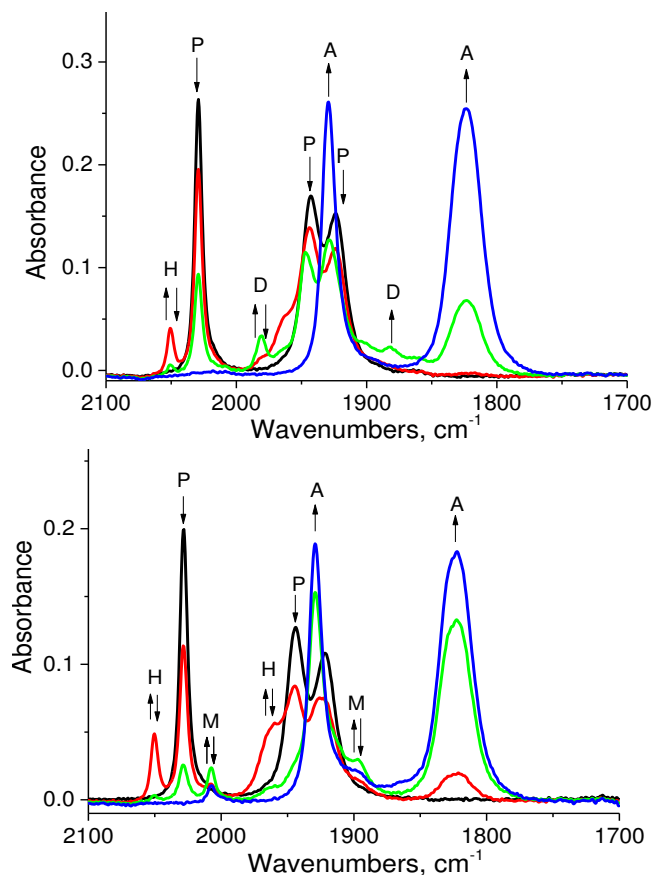


Figure 9. IR spectral changes accompanying in situ reduction of the complexes in Ar-saturated acetonitrile/0.2M $[\text{Bu}_4\text{N}][\text{PF}_6]$ within an OTTLE cell.

Top panel: MnIPIIMP, concurrent formation of a dimer and a 5-coordinate anion on reduction of the parent complex is observed. (P) $[\text{MnBr}(\text{CO})_3(\text{IPIIMP})]$; (D) $[\text{Mn}(\text{CO})_3(\text{IPIIMP})]_2$; (A) $[\text{Mn}(\text{CO})_3(\text{IPIIMP})]^-$; (H) $[\text{Mn}(\text{CO})_3(\text{H}_2\text{O})(\text{IPIIMP})]^+$. Bottom panel: MnDIPIMP, reduction of parent complex to 5-coordinate anion is observed. (P) $[\text{MnBr}(\text{CO})_3(\text{DIPIMP})]$; (A) $[\text{Mn}(\text{CO})_3(\text{DIPIMP})]^-$; (H) $[\text{Mn}(\text{CO})_3(\text{H}_2\text{O})(\text{DIPIMP})]^+$; (M) $[\text{Mn}(\text{CO})_3(\text{MeCN})(\text{DIPIMP})]^*$.

MnTBIMP shows an intermediate behavior to MnTBIEP and MnIPIIMP: similarly to MnTBIEP, the ^iBu substituent prevent dimer formation upon reduction; however, differently to MnTBIEP, and similar to MnIPIIMP, a rapid reaction with CO_2 takes place, which in case of MnTBIEP is considerably slowed down by the $\text{R} = \text{Me}$ group. It is important to note that if Mn–Mn dimer is reduced at the same, or even less negative potentials, than the parent complex, it will not be detected in

the studies.⁹ Thus the comments above regarding the absence of dimer formation only relate to the Br-complexes studied here. Substituting Br^- with a different group, which would lead to the parent complex being reduced at less negative potentials, may permit to detect these species. Five-coordinate complex formation appears to correlate with a less negative first reduction potential (see Table 3). A comparable correlation was found for Mn–R–DAB complexes and sterically hindered 2,2'-bipyridines already reported in the literature. These complexes also exhibit less negative 1st reduction potentials in comparison to their less sterically hindered counterparts, and form five-coordinate anions directly upon reduction.^{8,25}

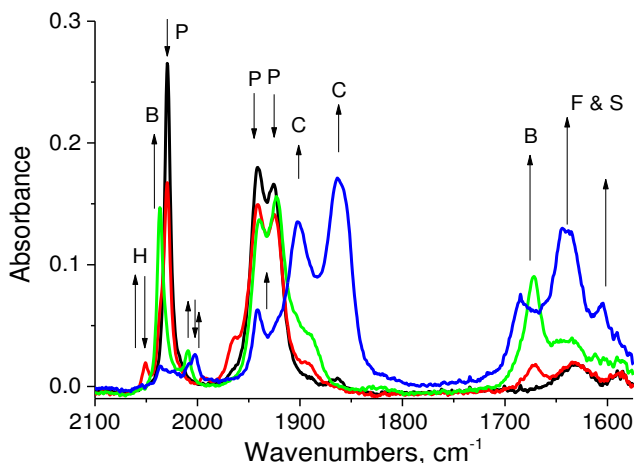


Figure 10. IR spectral changes accompanying in situ reduction of MnIMP ($[\text{MnBr}(\text{CO})_3(\text{IMP})]$) in CO_2 -saturated acetonitrile/0.2M $[\text{Bu}_4\text{N}][\text{PF}_6]$ within an OTTLE cell. (P) $[\text{MnBr}(\text{CO})_3(\text{IMP})]$; (B) $[\text{Mn}(\text{CO})_3(\text{IMP})(\eta^1\text{-OCO}_2\text{H})]$; (C) $[\text{Mn}(\text{CO})_3]^-$; (H) $[\text{Mn}(\text{CO})_3(\text{H}_2\text{O})(\text{IMP})]^+$; (F & S) free bicarbonate (OCO_2H^-) and subordinate formate (OCHO^-) accompanying the catalytic reduction of CO_2 to CO.

IR and UV-vis Spectroelectrochemistry under CO_2 Atmosphere

Electrochemical behaviour under a CO_2 atmosphere is vastly different to that under N_2 or Ar atmosphere. The electrocatalytic reduction of CO_2 with the four Mn complexes can be described in terms of three different types of behavior, largely controlled by the steric hindrance of the active imino $\text{C}=\text{N}$ bond. The MnIMP and MnIPIIMP are relatively unhindered and the catalytic behavior is almost identical. The initial reduction of parent and/or the cationic aqua complex results in the formation of the 2-electron reduced five-coordinate anion that reacts efficiently with CO_2 , no dimer is observed during the reduction of MnIMP (Figure 10) or MnIPIIMP (Figure 11).

The catalytic process at the initial cathodic wave is however inhibited by the rapid formation of a stable bicarbonate complex, absorbing at $2036, 1940, 1924$ and 1671 cm^{-1} for the IPIIMP, in line with the reports for sterically hindered Mn–mesityl-bipyridine²⁵ complexes and Mn–R–DAB complexes⁸. Further negative potential shift of ca. 0.7 V is needed to reduce the bicarbonate complex, resulting in the recovery of the five-coordinate anion that triggers the catalytic conversion of CO_2 .

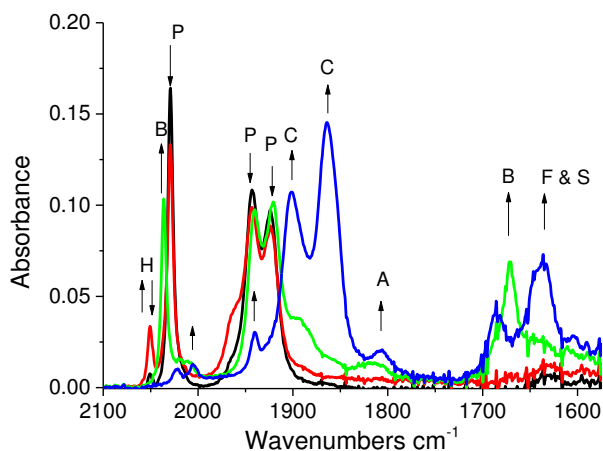


Figure 11. IR spectral changes accompanying in situ reduction of MnIPIMP ($[\text{MnBr}(\text{CO})_3(\text{IPIMP})]$) in CO_2 -saturated acetonitrile / 0.2M $[\text{Bu}_4\text{N}][\text{PF}_6]$ in an OTTLE cell. (P) $[\text{MnBr}(\text{CO})_3(\text{IPIMP})]$; (A) $[\text{Mn}(\text{CO})_3(\text{IPIMP})]$; (B) $[\text{Mn}(\text{CO})_3(\text{IPIMP})(\eta^1\text{-OCO}_2\text{H})]$; (C) $[\text{Mn}(\text{CO})_5]$; (H) $[\text{Mn}(\text{CO})_3(\text{H}_2\text{O})(\text{IPIMP})]^+$; (F & S) free bicarbonate (OCO_2H^-), subordinate formate (OCHO^-) accompanying the catalytic reduction of CO_2 to CO .

For the non-hindered IMP and IPIMP ligands the five-coordinate anion reacts rapidly and is not observed in the IR spectra on this timescale (for IMP) and only at a low concentration (for IPIMP). The production of CO in the thin-solution layer results in the displacement of the α -diimine ligand in the five-coordinate anion, forming the pentacarbonyl species $[\text{Mn}(\text{CO})_5]$ clearly seen in the IR spectra via the growth of bands at 1897 and 1865 cm^{-1} (species "C" in Figs 10-13). Remarkably, in these two cases only comparatively small amount of free bicarbonate or free formate (1685, 1638 and 1604 cm^{-1} for the IPIMP species) relative to $[\text{Mn}(\text{CO})_5]$ is observed, marking the high catalytic efficiency towards CO production.

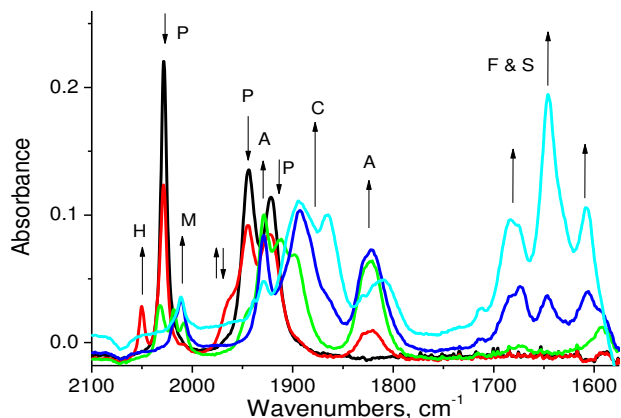


Figure 12. IR spectral changes accompanying in situ reduction of MnDIPIMP in CO_2 -saturated acetonitrile / 0.2M $[\text{Bu}_4\text{N}][\text{PF}_6]$ within an OTTLE cell. (P) $[\text{MnBr}(\text{CO})_3(\text{DIPIMP})]$; (A) $[\text{Mn}(\text{CO})_3(\text{DIPIMP})]$; (B) $[\text{Mn}(\text{CO})_3(\text{DIPIMP})(\eta^1\text{-OCO}_2\text{H})]$; (H) aqua-complex $[\text{Mn}(\text{CO})_3(\text{H}_2\text{O})(\text{DIPIMP})]^+$; (C) $[\text{Mn}(\text{CO})_5]$; (M) $[\text{Mn}(\text{CO})_3(\text{MeCN})(\text{DIPIMP})]^+$; (F & S) free bicarbonate (OCO_2H^-) and subordinate formate (OCHO^-).

Upon reduction of the more C=N-hindered DIPIMP complex, the five-coordinate anion formed does not react with CO_2 efficiently and a metastable population of the anionic five-coordinate MnDIPIMP species, $[\text{Mn}(\text{CO})_3(\text{DIPIMP})]^-$, is detected even under high excess of CO_2 . Interestingly, and differently from the other complexes in the Mn-IP series, the formation of a bicarbonate complex is only detected at the potential corresponding to the reduction of CO_2 -associated species at around -2 V vs Fc/Fc^+ , whilst prior coordination of CO_2 to the five-coordinate anion at the parent MnDIPIMP cathodic wave no bicarbonate ligand signature not detected. At the catalytic potential where the bicarbonate complex is reduced the conversion of CO_2 to CO is also inefficient. High concentration of the five-coordinate anion is still seen, converting slowly to $[\text{Mn}(\text{CO})_5]$ when the concentration of CO increases; at the same time the production of free bicarbonate (and free formate) is much higher compared to the MnIMP and MnIPIMP cases, marking the low catalytic efficiency toward CO production. Notably, the lower CO -stretching band of $[\text{Mn}(\text{CO})_3(\text{DIPIMP})]^-$ becomes shifted from its standard position (1829/2 cm^{-1}) to lower energy (ca. 1810 cm^{-1}) at the advanced stage of the catalytic conversion. This shift may indicate the presence of an observable adduct of the five-coordinate anion, most likely with CO_2 or formate (over the Mn-N=C bond). In this context it is interesting to note that the related Re-IP complex³⁷ forms the carbonate complex in two 1e-reduction steps, via a direct coordination to the Re center, without C=N being directly involved.

In the case of MnTBIEP the imino C=N bond is hindered both at the carbon atom via the methyl group and by the t-butyl group on the phenyl moiety. There are similarities but also differences with the hindered DIPIMP complex, which does not have a hindering group at the C-atom of the imino C=N moiety. Upon reduction of the parent complex in CO_2 saturated acetonitrile the five-coordinate anion $[\text{Mn}(\text{CO})_3(\text{TBIEP})]^-$ coordinates CO_2 forming the bicarbonate complex readily (similar to IMP and IPIMP) with the characteristic IR absorption band at 1673 cm^{-1} .^{8,30}

A small amount of the five-coordinate anion $[\text{Mn}(\text{CO})_3(\text{TBIEP})]^-$ is observed in the initial step. Lowering the potential to around -1.5 V vs Fc/Fc^+ results in catalytic conversion of the bicarbonate complex, however, similar to MnDIPIMP this conversion is not efficient compared with MnIMP and MnIPIMP. This is shown via the slower growth of $[\text{Mn}(\text{CO})_5]$ compared to IPIMP and the greater quantities of free bicarbonate produced. As with MnDIPIMP the five-coordinate anion 'adduct' form is observed with the lower energy CO -stretching band shifted to a lower wavenumber (from 1814 to 1803 cm^{-1}). Thus, hindering the imine C atom does not affect adduct formation between CO_2 and $[\text{Mn}(\text{CO})_3(\text{TBIEP})]^-$.

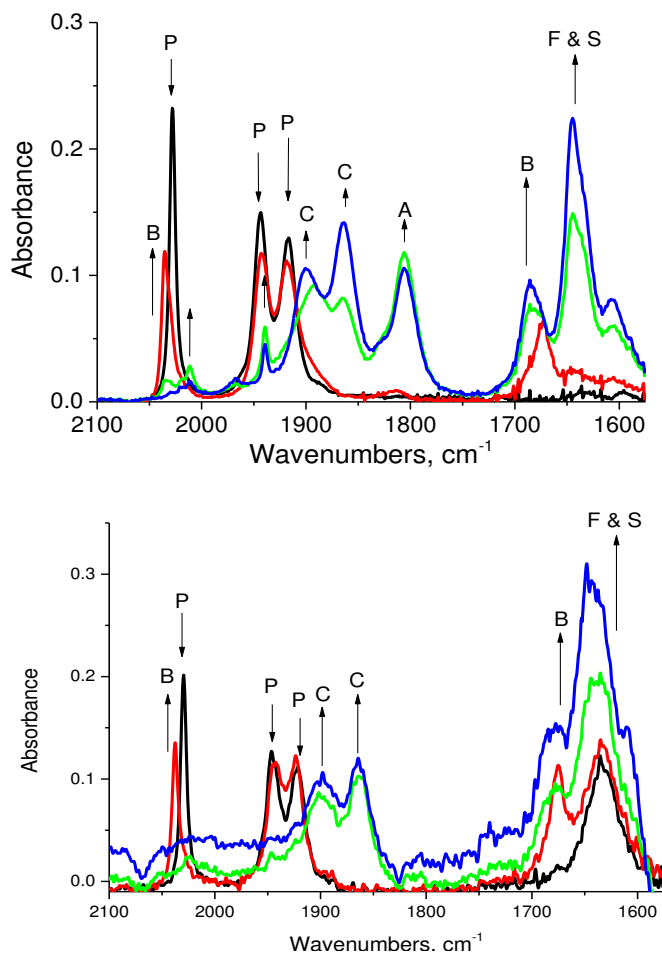


Figure 13. IR spectral changes accompanying in situ reduction of complexes in CO₂-saturated acetonitrile/0.2 M [Bu₄N][PF₆] within an OTTLE cell. Top panel: For MnTBIEP, (P) [MnBr(CO)₃(TBIEP)]; (A) [Mn(CO)₃(TBIEP)]; (B) [Mn(CO)₃(TBIEP)(η¹-OCO₂H)]; (C) [Mn(CO)₃]⁻; (F & S) free bicarbonate (OCO₂H⁻) and formate (OCHO⁻) accompanying the catalytic reduction of CO₂ to CO. Bottom panel: For MnTBIMP, (P) [MnBr(CO)₃(TBIMP)]; (B) [Mn(CO)₃(TBIMP)(η¹-OCO₂H)]; (C) [Mn(CO)₃]⁻; (F & S) free bicarbonate (OCO₂H⁻) and formate (OCHO⁻) accompanying the catalytic reduction of CO₂ to CO.

However, at the negative potentials where the bicarbonate complex is reduced (recovering the catalytic five-coordinate anion) the hindrance provided by the methyl and ^tbutyl groups also negatively affects the catalytic formation of CO₂ to CO (as evidenced by large amounts of free bicarbonate and slow formation of [Mn(CO)₃]⁻ at lower CO concentration). It is not very clear whether this greater hindrance is due directly to the presence of the methyl group on the C position or whether this is due to the ^t-butyl group inhibiting rotation of the phenyl moiety and preventing the five-coordinate anion from adopting a more suitable (pyramidal) geometry for CO₂ association.

Again, MnTBIMP behaves in a similar fashion to MnTBIEP. Upon reduction the parent complex rapidly associates CO₂ forming the bicarbonate complex, as the reduction potential is lowered further the bicarbonate complex is reduced forming

CO which is able to displace the TBIMP and forming [Mn(CO)₃]⁻. One important difference is that significantly less (if any) five-coordinate anion is observed in the presence of CO₂ than was the case with both MnTBIEP and MnDIPIMP. This suggests that ^tBu is not as sterically demanding as two ⁱPr groups in these systems as CO₂ is still able to coordinate.

Estimation of Electrocatalytic Activity towards CO Production Using Gas Chromatography

The CO concentration as a function of time in the course of controlled potential electrolysis estimated by GC analysis of the head-space of the electrolysis cell shows a gradual build-up of CO in the course of the electrolysis (Fig. S119). A comparison with the performance of [MnBr(CO)₃(bpy)] catalyst investigated under identical conditions (see Fig S19) that the efficiency of CO production for the new catalysts **1-5** is comparable to that of [MnBr(CO)₃(bpy)], with the least sterically hindered, MnIMP complex being somewhat more efficient. Due to the large volumes used in the experiment, considerable secondary processes occur during bulk electrolysis, manifested in the loss of the initial intense yellow/red color of the solution as the reaction progressed, which was concomitant with an increase in current towards the end of the electrolysis. These deviations from an ideal behavior suggests that as CO₂ is depleted in solution, competing catalyst degradation pathways begin to occur, precluding reliable estimates of efficiencies.

Estimation of efficiency from the CV data was done by the relative i_{cat}/i_p values (Table S1) following the method described in ref.^{4,7} Comparing the current values detected in the CV at -2.24V (vs. Fc/Fc⁺) recorded under CO₂ and N₂ atmosphere in acetonitrile/water also show that the performance of **1-5** is comparable to one another, and is comparable to that of [Mn(CO)₃(bpy)Br], at 30-60% efficiency. It is important that most sterically protected, MnDIPIMP and MnTBIEP, seem to be performing better as far as i_{cat}/i_p are concerned, but that the least sterically hindered MnIMP is the most efficient in the series. These observations are different to the observation of the MnTBIMP producing more CO than [Mn(bpy)(CO)₃Br] in the bulk electrolysis/GC experiments. Whilst these data can only be considered in relative terms, they do show the potential of these complexes to act as a test-bed for optimizing steric vs. electronic effects in CO₂ reduction, whereby the thermodynamic factors, the rate of CO₂ coordination, and the rate of decomposition of catalyst precursor species, need to be balanced.

The main transformation pathways of **1-5** upon reduction under inert atmosphere, and under atmosphere of CO₂, are summarised schematically in Fig. 14.

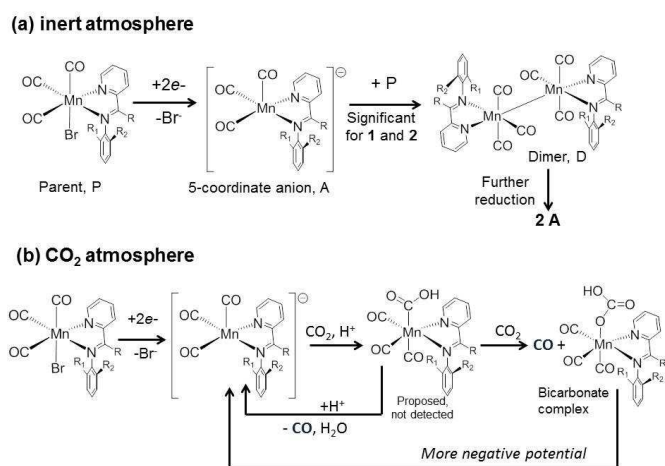


Figure 14. The main transformation pathways of **1-5** upon reduction under (a) inert atmosphere, and (b) under atmosphere of CO_2 . [A] is detected for (**3**) only due to comparatively slower reaction of [**3**] with CO_2 .

Conclusions

A series of Mn(I) tricarbonyl electrocatalysts for CO_2 reduction, which employ, for the first time, asymmetric α -diimine ligands, imino-pyridines, has been developed, and their catalytic activity confirmed and evaluated in detail.

We have demonstrated through conventional and thin-layer cyclic voltammetry, UV-vis and IR spectroscopy and DFT computational analysis the π -decoupling of the phenyl from the Mn(pyridine-CCN) metallacycle. The practical effect of this feature is the ability to disentangle steric and electronic effects of the α -diimine ligand on the catalytic properties. Until now, introduction of sterically bulky groups, which are also typically electron donating, was coming at a price of the increased overpotential required for CO_2 reduction. The use of asymmetric α -diimine has allowed us to probe the effect of adding ever greater sterically demanding groups without much change in the catalytic potential. We have demonstrated that systematic increase in the steric hindrance of the R_1 & R_2 in the IMP sub-series results in the switch of the nature of the first reduction product detected on the timescale of the experiment under an inert gas atmosphere, from a dimer to a five-coordinate anion, at the very similar reduction potential. In the absence of sterically hindering groups on the phenyl ring, MnIMP, a dimer is formed, whilst increasing the steric hindrance by adding ^iPr groups to the R_1 and R_2 positions (MnDIPIMP) resulted in direct formation of the five-coordinate anion in line with prior observations from similar sterically hindered ligands.^{23,26} MnIPIMP (in which case the dimer may be reduced at the parent cathodic wave due to slightly negatively shifted reduction potential vs. that for MnIMP) exhibited intermediate behavior to MnIMP and MnDIPIMP with both the dimer, and the five-coordinate anion observed forming concurrently. MnTBIMP and MnTBIEP both formed the five-coordinate anion directly upon reduction of the parent complex.

Under CO_2 atmosphere, all of the complexes reduce CO_2 to CO. The buildup of CO in the thin-layer spectro-electrochemical cell resulted in the displacement of the α -diimine ligand forming $[\text{Mn}(\text{CO})_5]$. The complex containing the most sterically demanding ligand DIPIMP is, as anticipated, least susceptible to α -diimine displacement with CO, forming exclusively the five-coordinate anion upon the first reduction; it also has least propensity to coordinating CO_2 , resulting in a considerable build-up of the concentration of the five-coordinate anion. An intermediate formation of the bicarbonate is also likely as the band at 1686 cm^{-1} is present at intermediate times. Of particular interest is that least sterically hindered MnIMP seemed to form a CO_2 associated complex directly upon the first reduction, with no significant formation of the dimer being observed on the timescale of the experiment. This behavior is similar to that reported for the symmetric non-aromatic Mn-R-DAB ($R = \text{alkyl}$) compounds.^{8,30} The formation of a stable bicarbonate complex, either through the coordination to the metal center or via the imino $\text{C}=\text{N}$ bond^{23,37} leads to the need of increased overpotential. From that point of view, the steric hindering (protection) of the metal center/the imino $\text{C}=\text{N}$ bond in the Mn(IP) complexes is advantageous as it disfavors the Mn-Mn dimerization (when comparing MnIMP with MnDIPIMP). However, such steric crowding also slows down the catalytic conversion of CO_2 to CO at the negative overpotentials, as can be seen in the GC data and from the i_{cat}/i_p values. A difference in the reactivity of MnTBIMP and MnTBIEP, where no dimer formation has been detected for either of the complexes in the IR-SEC experiments, but where MnTBIEP exhibits slower CO_2 conversion due to $R=\text{CH}_3$ alters the HOMO-LUMO gap in comparison to the 'IMP' series, as well as introducing additional steric bulk, further supports the notion that it is possible to separate steric and electronic factors to a large extent. Balancing these factors by careful ligand design may lead to the optimal solution.

The new family of CO_2 reduction catalysts presents an exciting platform for versatile and relatively independent tuning of steric and electronic properties, offering a far greater tuneability than catalysts with aromatic bpy-based or non-aromatic R-DAB-based ligands, and abundant options to refine and optimize Mn tricarbonyl CO_2 reduction catalysts.

ASSOCIATED CONTENT

Calculated frontier orbitals from HOMO-3 to LUMO+3 for all studied complexes, .cif files of crystal structures, complete CV, control experiments, and ^1H NMR spectra of the new complexes. This material is available free of charge via the Internet at <http://pubs.acs.org>.

AUTHOR INFORMATION

Corresponding Authors

Julia.Weinstein@sheffield.ac.uk; F.Hartl@reading.ac.uk

Author Contributions

All authors approved the final version of the manuscript.

ACKNOWLEDGMENTS

The authors are grateful to E. J. Carrington, T. M. Roseveare and C. M. Kiker for assistance in interpreting the X-ray diffraction data, Drs A. Haynes and S. Parker for discussions, and G. Chandrakumar for experimental assistance. Support of the University of Sheffield and its SURE scheme, Shine DTC, the University of Reading (Project D14-015), the EPSRC, and the RSC Undergraduate Bursary (TK and HF) is gratefully acknowledged.

REFERENCES

- Morris, A. J.; Meyer, G. J.; Fujita, E. Molecular Approaches to the Photocatalytic Reduction of Carbon Dioxide for Solar Fuels. *Acc. Chem. Res.*, **2009**, *42*, 1983-1994.
- Bourrez, M.; Molton, F.; Chardon-Noblat, S.; Deronzier, A. [Mn(bipyridyl)(CO)₃Br]: An Abundant Metal Carbonyl Complex as Efficient Electrocatalyst for CO₂ Reduction. *Angew. Chem. Int. Ed.* **2011**, *50*, 9903-9906.
- Hawecker, J.; Lehn, J.-M.; Ziesel, R. Electrocatalytic Reduction of Carbon Dioxide Mediated by Re(bipy)(CO)₃Cl (bipy = 2,2'-bipyridine). *J. Chem. Soc., Chem. Commun.* **1984**, 328-330.
- Smieja, J. M.; Benson, E. E.; Kumar, B.; Grice, K. A.; Seu, C. S.; Miller, A. J. M.; Mayer, J. M.; Kubiak, C. P. Kinetic and structural studies, origins of selectivity, and interfacial charge transfer in the artificial photosynthesis of CO. *Proc. Natl. Acad. Sci. U. S. A.* **2012**, *109*, 15646-15650.
- Grice, K. A.; Kubiak, C. P. Recent Studies of Rhenium and Manganese Bipyridine Carbonyl Catalysts for the Electrochemical Reduction of CO₂. In *Advances in Inorganic Chemistry*; **2014**, Vol. 66, Ed. M. Aresta. pp. 163-188; Aresta, M., Dibenedetto, A.; Angelini, A. Converting "Exhaust" Carbon into "Working" Carbon, *ibid.*, pp. 259-288.
- Wong, K.; Chung, W.; Lau, C. The effect of weak Brønsted acids on the electrocatalytic reduction of carbon dioxide by a rhenium tricarbonyl bipyridyl complex. *J. Electroanal. Chem.* **1998**, *453*, 161-170.
- Smieja, J. M.; Sampson, M. D.; Grice, K. A.; Benson, E. E.; Froehlich, J. D.; Kubiak, C. P. Manganese as a Substitute for Rhenium in CO₂ Reduction Catalysts: The Importance of Acids. *Inorg. Chem.* **2013**, *52*, 2484-2491.
- Zeng, Q.; Tory, J.; Hartl, F. Electrocatalytic Reduction of Carbon Dioxide with a Manganese(I) Tricarbonyl Complex Containing a Nonaromatic α -Diimine Ligand. *Organometallics* **2014**, *33*, 5002-5008.
- Rossenaar, B. D.; Hartl, F.; Stufkens, D. J.; Amatore, C.; Maisonhaute, E.; Verpeaux, J.-N. Electrochemical and IR/UV-Vis Spectroelectrochemical Studies of fac-[Mn(X)(CO)₃(Pr-DAB)]ⁿ (n = 0, X = Br, Me, Bz; n = +1, X = THF, MeCN, nPrCN, P(OMe)₃; iPr-DAB = 1,4-Diisopropyl-1,4-diaza-1,3-butadiene) at Variable Temperatures: Relation between Electrochemical and Photochemical Generation of [Mn(CO)₃(α -diimine)]. *Organometallics* **1997**, *16*, 4675-4685.
- Grills, D. C.; Farrington, J. A.; Layne, B. H.; Lyman, S. V.; Mello, B. A.; Preses, J. M.; Wishart, J. F. Mechanism of the Formation of a Mn-Based CO₂ Reduction Catalyst Revealed by Pulse Radiolysis with Time-Resolved Infrared Detection. *J. Am. Chem. Soc.* **2014**, *136*, 5563-5566.
- Johnson, F. P. A.; George, M. W.; Hartl, F.; Turner, J. J. Electrocatalytic Reduction of CO₂ Using the Complexes [Re(bpy)(CO)₃L]ⁿ (n = +1, L = P(OEt)₃, CH₃CN; n = 0, L = Cl⁻, Otf⁻; bpy = 2,2'-Bipyridine; Otf = CF₃SO₃) as Catalyst Precursors: Infrared Spectroelectrochemical Investigation. *Organometallics* **1996**, *15*, 3374-3387.
- Smieja, J. M.; Kubiak, C. P. Inorg. Chem. Re(bipy-^tBu)(CO)₃Cl-improved Catalytic Activity for Reduction of Carbon Dioxide: IR-Spectroelectrochemical and Mechanistic Studies. **2010**, *49*, 9283-9289.
- Machan, C. W.; Sampson, M. D.; Chabolla, S. A.; Dang, T.; Kubiak, P. Developing a Mechanistic Understanding of Molecular Electrocatalysts for CO₂ Reduction using Infrared Spectroelectrochemistry. *Organometallics* **2014**, *33*, 4550-4559.
- Cabeza, J. A.; Garcia-Alvarez, P.; Gobetto, R.; Gonzalez-Alvarez, L.; Nervi, C.; Perez-Carreno, E.; Polo, D. [MnBrL(CO)₄] (L = Amidinatogermylene): Reductive Dimerization, Carbonyl Substitution, and Hydrolysis Reactions. *Organometallics* **2016**, *35*, 1761-1770.
- Machan, C. W.; Stanton, C. J.; Vandezande, J. E.; Majetich, G. F.; Schaefer, H. F.; Kubiak, C. P.; Agarwal, J. Electrocatalytic Reduction of Carbon Dioxide by Mn(CN)(2,2'-bipyridine)(CO)₃: CN Coordination Alters Mechanism. *Inorg. Chem.* **2015**, *54*, 8849-8856.
- Sieh, D.; Kubiak, C. P. A Series of Diamagnetic Pyridine Monoimine Rhenium Complexes with Different Degrees of Metal-to-Ligand Charge Transfer: Correlating ¹³C NMR Chemical Shifts with Bond Lengths in Redox-Active Ligands. *Chem. Eur. J.* **2016**, *22*, 10638-10650.
- Riplinger, C.; Sampson, M. D.; Ritzmann, A. M.; Kubiak, C. P.; Carter, E. A. Mechanistic Contrasts between Manganese and Rhenium Bipyridine Electrocatalysts for the Reduction of Carbon Dioxide. *J. Am. Chem. Soc.* **2014**, *136*, 16285-16298.
- Franco, F.; Cometto, C.; Ferrero Vallana, F.; Sordello, F.; Priola, E.; Minero, C.; Nervi, C.; Gobetto, R. A local proton source in a [Mn(bpy-R)(CO)₃Br]-type redox catalyst enables CO₂ reduction even in the absence of Brønsted acids. *Chem. Commun.* **2014**, *50*, 14670-14673.
- Bourrez, M.; Orio, M.; Molton, F.; Vezin, H.; Duboc, C.; Deronzier, A.; Chardon-Noblat, S. Pulsed-EPR Evidence of a Manganese(II) Hydroxycarbonyl Intermediate in the Electrocatalytic Reduction of Carbon Dioxide by a Manganese Bipyridyl Derivative. *Angew. Chem. Int. Ed.* **2014**, *53*, 240-243.
- Sullivan, B. P.; Bolinger, C. M.; Conrad, D.; Vining, W. J.; Meyer, T. J. One- and Two-electron Pathways in the Electrocatalytic Reduction of CO₂ by fac-Re(bpy)(CO)₃Cl (bpy = 2,2'-bipyridine). *J. Chem. Soc., Chem. Commun.* **1985**, 1414-1416.
- Stor, G. J.; Hartl, F.; van Outersterp, J. W. M.; Stufkens,

- D. J. Spectroelectrochemical (IR, UV/Vis) Determination of the Reduction Pathways for a Series of $[\text{Re}(\text{CO})_3(\alpha\text{-diimine})\text{L}]^{0/+}$ (L' = Halide, Otf, THF, MeCN, n-PrCN, PPh_3 , $\text{P}(\text{OMe})_3$) Complexes. *Organometallics*, **1995**, 14, 1115-1131.
- (22) Walsh, J. J.; Smith, C. L.; Neri, G.; Whitehead, G. F. S.; Robertson, C. M.; Cowan, A. J. Improving the efficiency of electrochemical CO_2 reduction using immobilized manganese complexes. *Faraday Dis.* **2015**, 183, 147-160.
- (23) Stor, G. J.; Morrison, S. L.; Stufkens, D. J.; Oskam, A. The Remarkable Photochemistry of $\text{fac-XMn}(\text{CO})_3(\alpha\text{-diimine})$ (X = Halide): Formation of $\text{Mn}_2(\text{CO})_6(\alpha\text{-diimine})_2$ via the mer Isomer and Photocatalytic Substitution of X^- in the Presence of PR_3 . *Organometallics* **1994**, 13, 2641-2650.
- (24) Sampson, M. D.; Kubiak, C. P. Electrocatalytic Dihydrogen Production by an Earth-Abundant Manganese Bipyridine Catalyst. *Inorg. Chem.* **2015**, 54, 6674-6676.
- (25) Sampson, M. D.; Nguyen, A. D.; Grice, K. A.; Moore, C. E.; Rheingold, A. L.; Kubiak, C. P. Manganese Catalysts with Bulky Bipyridine Ligands for the Electrocatalytic Reduction of Carbon Dioxide: Eliminating Dimerization and Altering Catalysis. *J. Am. Chem. Soc.* **2014**, 136, 5460-5471.
- (26) Agarwal, J.; Shaw, T. W.; Stanton III, C. J.; Majetich, G. F.; Bocarsly, A. B.; Schaefer III, H. F. NHC-Containing Manganese(I) Electrocatalysts for the Two-Electron Reduction of CO_2 . *Angew. Chemie Int. Ed.* **2014**, 126, 5252-5255.
- (27) Costentin, C.; Robert, M.; Savéant, J.-M. Catalysis of the electrochemical reduction of carbon dioxide. *Chem. Soc. Rev.* **2013**, 42, 2423-2436.
- (28) Sampson, M. D.; Kubiak, C. P. Manganese Electrocatalysts with Bulky Bipyridine Ligands: Utilizing Lewis Acids To Promote Carbon Dioxide Reduction at Low Overpotentials. *J. Am. Chem. Soc.* **2016**, 138, 1386-1393.
- (29) Lam, Y. C.; Nielsen, R. J.; Gray, H. B.; Goddard, W. A. A Mn Bipyrimidine Catalyst Predicted To Reduce CO_2 at Lower Overpotential. *ACS Catal.* **2015**, 5, 2521-2528.
- (30) Vollmer, M. V.; Machan, C. W.; Clark, M. L.; Antholine, W. E.; Agarwal, J.; Schaefer, H. F.; Kubiak, C. P.; Walensky, J. R. Synthesis, Spectroscopy, and Electrochemistry of $(\alpha\text{-Diimine})\text{M}(\text{CO})_3\text{Br}$, M = Mn, Re, Complexes: Ligands Isoelectronic to Bipyridyl Show Differences in CO_2 Reduction. *Organometallics* **2014**, 34, 3-12.
- (31) Agarwal, J.; Shaw, T. W.; Schaefer III, H. F.; Bocarsly, A. B. Design of a Catalytic Active Site for Electrochemical CO_2 Reduction with Mn(I) Tri-carbonyl Species. *Inorg. Chem.* **2015**, 54, 5285-5294.
- (32) Stufkens, D. J.; van Outersterp, J. W. M.; Oskam, A.; Rossenaar, B. D.; Stor, G. J. The photochemical formation of organometallic radicals from α -diimine complexes having a metal-metal, metal-alkyl or metal-halide bond. *Coord. Chem. Rev.* **1994**, 132, 147-154.
- (33) Rossenaar, B. D.; Kleverlaan, C. J.; van der Ven, M. C. E.; Stufkens, D. J.; Oskam, A.; Fraanje, J.; Goubitz, K. Synthesis and spectroscopic properties of $\text{Re}(\text{R})(\text{CO})_3(\alpha\text{-diimine})$ (R = alkyl; α -diimine = R'-pyCa, R'-DAB) complexes. Crystal structure of $\text{Re}(\text{Me})(\text{CO})_3(\text{Pr-DAB})$. *J. Organomet. Chem.* **1995**, 493, 153-162.
- (34) Sieh, D.; Lacy, D. C.; Peters, J. C.; Kubiak, C. P. Reduction of CO_2 by Pyridine Monoimine Molybdenum Carbonyl Complexes: Cooperative Metal-Ligand Binding of CO_2 . *Chem. Eur. J.* **2015**, 21, 8497-8503.
- (35) Gonsalvi, L.; Gaunt, J. A.; Adams, H.; Castro, A.; Sunley, G. J.; Haynes, A. Quantifying Steric Effects of α -Diimine Ligands. Oxidative Addition of MeI to Rhodium(I) and Migratory Insertion in Rhodium(III) Complexes. *Organometallics* **2003**, 22, 1047-1054.
- (36) Machan, C. W.; Chabolla, S. A.; Kubiak, C. P. Reductive Disproportionation of Carbon Dioxide by an Alkyl-Functionalized Pyridine Monoimine Re(I) fac-Tricarbonyl Electrocatalyst. *Organometallics* **2015**, 34, 4678-4683.
- (37) Alvarez, C. M.; García-Rodríguez, R.; Miguel, D. Carbonyl complexes of manganese, rhenium and molybdenum with ethynyliminopyridine ligands. *J. Organomet. Chem.* **2007**, 692, 5717-5726.
- (38) Alvarez, C. M.; García-Rodríguez, R.; Miguel, D. Pyridine-2-carboxaldehyde as ligand: Synthesis and derivatization of carbonyl complexes. *Dalton Trans.* **2007**, 3546-3554.
- (39) Bond, M.; Grabaric, B. S.; Grabaric, Z. Kinetic and Thermodynamic Study of Reactions of Some Substituted Manganese(I) and Manganese(II) Tricarbonyl Complexes Using Spectrophotometric and Electrochemical Techniques. *Inorg. Chem.* **1978**, 17, 1013-1018.
- (40) Krause, L.; Herbst-Irmer, R.; Sheldrick, G. M.; Stalke, D. Comparison of silver and molybdenum microfocus X-ray sources for single-crystal structure determination. *J. Appl. Crystallogr.* **2015**, 48, 3-10.
- (41) Frisch, M. J.; Trucks, G. W.; Schlegel, H. B.; Scuseria, G. E.; Robb, M. A.; Cheeseman, J. R.; Scalmani, G.; Barone, V.; Mennucci, B.; Petersson, G. A.; Nakatsuji, H.; Caricato, M.; Li, X.; Hratchian, H. P.; Izmaylov, A. F.; Bloino, J.; Zheng, G.; Sonnenberg, J. L.; Hada, M.; Ehara, M.; Toyota, K.; Fukuda, R.; Hasegawa, J.; Ishida, M.; Nakajima, T.; Honda, Y.; Kitao, O.; Nakai, H.; Vreven, T.; Montgomery Jr., J. A.; Peralta, J. E.; Ogliaro, F.; Bearpark, M.; Heyd, J. J.; Brothers, E.; Kudin, K. N.; Staroverov, V. N.; Kobayashi, R.; Normand, J.; Raghavachari, K.; Rendell, A.; Burant, J. C.; Iyengar, S. S.; Tomasi, J.; Cossi, M.; Rega, N.; Millam, J. M.; Klene, M.; Knox, J. E.; Cross, J. B.; Bakken, V.; Adamo, C.; Jaramillo, J.; Gomperts, R.; Stratmann, R. E.; Yazyev, O.; Austin, A. J.; Cammi, R.; Pomelli, C.; Ochterski, J. W.; Martin, R. L.; Morokuma, K.; Zakrzewski, V. G.; Voth, G. A.; Salvador, P.; Dannenberg, J. J.; Dapprich, S.; Daniels, A. D.; Farkas, Ö.; Foresman, J. B.; Ortiz, J. V.; Cioslowski, J.; Fox, D. J. Gaussian 09, Revision D.01, Gaussian, Inc., Wallingford CT, 2013.

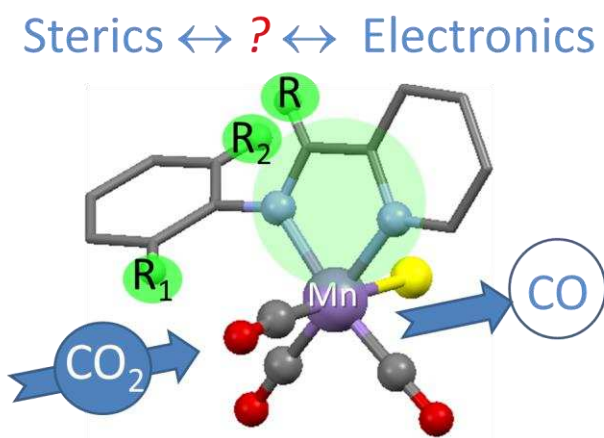
- (42) Becke, A. D. Density-functional thermochemistry. III. The role of exact exchange. *J. Chem. Phys.* **1993**, *98*, 5648-5652.
- (43) Lee, C.; Yang, W.; Parr, R. G. Development of the Colle-Salvetti correlation-energy formula into a functional of the electron density. *Phys. Rev B.* **1988**, *37*, 785-789.
- (44) Nicklass, A.; Dolg, M.; Stoll, H.; Preuss, H. Ab initio energy-adjusted pseudopotentials for the noble gases Ne through Xe: Calculation of atomic dipole and quadrupole polarizabilities. *J. Chem. Phys.* **1995**, *102*, 8942-8952.
- (45) Dunning Jr., T. H.; Hay, P. J. in 'Modern Theoretical Chemistry', Vol. 3, Schaefer, H. F., Ed. Plenum Press, New York 1977.
- (46) Krishnan, R.; Binkley, J. S.; Seeger, R.; Pople, J. A. Self-consistent molecular orbital methods. XX. A basis set for correlated wave functions. *J. Chem. Phys.* **1980**, *72*, 650-654.
- (47) McLean, A. D.; Chandler, G. S. Contracted Gaussian basis sets for molecular calculations. I. Second row atoms, $Z=11-18$. *J. Chem. Phys.* **1980**, *72*, 5639-5648.
- (48) Mennucci, B.; Tomasi, J. Continuum solvation models: A new approach to the problem of solute's charge distribution and cavity boundaries. *J. Chem. Phys.* **1997**, *106*, 5151-5158.
- (49) Cossi, M.; Barone, V.; Mennucci, B.; Tomasi, J. Ab initio study of ionic solutions by a polarizable continuum dielectric model. *Chem. Phys. Lett.* **1998**, *286*, 253-260.
- (50) Bistoni, G.; Rampino, S.; Scafuri, N.; Ciancaleoni, G.; Zuccaccia, D.; Belpassi, L.; Tarantelli, F. How π back-donation quantitatively controls the CO stretching response in classical and non-classical metal carbonyl complexes. *Chem. Sci.* **2015**, *7*, 1174-1184.

Manganese tricarbonyl complexes with asymmetric α -diimine ligands, 2-imino-pyridines: towards decoupling steric and electronic factors in electrocatalytic CO₂ reduction

Steven J. P. Spall,¹ Theo Keane,¹ Joanne Tory,² Dean C. Cocker,¹ Harry Adams,¹ Anthony J. H. M. Meijer,¹ František Hartl^{2*} and Julia A. Weinstein^{1*}

¹Department of Chemistry, University of Sheffield, Sheffield, S3 7HF, UK;

²Department of Chemistry, University of Reading, Whiteknights, Reading RG6 6AD, UK



Electrocatalytic CO₂ reduction with Mn(I) tricarbonyl complexes:

How introducing steric bulk prevents unwanted side-reactions

without jeopardizing energy requirements in a family of catalysts with

“hybrid” diimine ligands, substituted phenyl-imino-pyridines.
